Title

Genome-wide transcriptional responses of osteoblasts to different titanium surface topographies.

Authors

Suzumura, Toshikatsu
Ogawa, Takahiro
Komatsu, Keiji
et al.

Publication Date

2023-12-01

DOI

10.1016/j.mtbio.2023.100852

Peer reviewed

Materials Today Bio 23 (2023) 100852

Contents lists available at ScienceDirect

Materials Today Bio

journal homepage: www.journals.elsevier.com/materials-today-bio

Genome-wide transcriptional responses of osteoblasts to different titanium surface topographies

Keiji Komatsu [a,b,*], Takanori Matsuura [a], Toshikatsu Suzumura [a], Takahiro Ogawa [a]

[a] Weintraub Center for Reconstructive Biotechnology and the Division of Regenerative and Reconstructive Sciences, UCLA School of Dentistry, Los Angeles, CA, 90095, USA

[b] Department of Lifetime Oral Health Care Sciences, Graduate School of Medical and Dental Sciences, Tokyo Medical and Dental University (TMDU), Tokyo, 113-8549, Japan

ARTICLE INFO

Keywords:
Titanium surface topography
Osteoblast differentiation
Transcriptional profile
Dental implant
Osseointegration

ABSTRACT

This is the first genome-wide transcriptional profiling study using RNA-sequencing to investigate osteoblast responses to different titanium surface topographies, specifically between machined, smooth and acid-etched, microrough surfaces. Rat femoral osteoblasts were cultured on machine-smooth and acid-etched microrough titanium disks. The culture system was validated through a series of assays confirming reduced osteoblast attachment, slower proliferation, and faster differentiation on microrough surfaces. RNA-sequencing analysis of osteoblasts at an early stage of culture revealed that gene expression was highly correlated ($r = 0.975$) between the two topographies, but 1.38 % genes were upregulated and 0.37 % were downregulated on microrough surfaces. Upregulated transcripts were enriched for immune system, plasma membrane, response to external stimulus, and positive regulation to stimulus processes. Structural mapping confirmed microrough surface-promoted gene sharing and networking in signaling pathways and immune system/responses. Target-specific pathway analysis revealed that Rho family G-protein signaling pathways and actin genes, responsible for the formation of stress fibers, cytoplasmic projections, and focal adhesion, were upregulated on microrough surfaces without upregulation of core genes triggered by cell-to-cell interactions. Furthermore, disulfide-linked or -targeted extracellular matrix (ECM) or membranous glycoproteins such as laminin, fibronectin, CD36, and thrombospondin were highly expressed on microrough surfaces. Finally, proliferating cell nuclear antigen (PCNA) and cyclin D1, whose co-expression reduces cell proliferation, were upregulated on microrough surfaces. Thus, osteoblasts on microrough surfaces were characterized by upregulation of genes related to a wide range of functions associated with the immune system, stress/stimulus responses, proliferation control, skeletal and cytoplasmic signaling, ECM-integrin receptor interactions, and ECM-membranous glycoprotein interactions, furthering our knowledge of the surface-dependent expression of osteoblastic biomarkers on titanium.

Credit author Statement

Keiji Komatsu: Conceptualization, Methodology, Software, Validation, Investigation, Data curation, Formal analysis, Visualization, Supervision, Writing – original draft, Writing – review & editing. **Takanori Matsuura:** Investigation, Methodology, Validation. **Toshikatsu Suzumura:** Investigation, Data curation. **Takahiro Ogawa:** Conceptualization, Resources, Funding acquisition, Writing – review & editing, Project administration.

1. Introduction

Despite a growing clinical need for faster healing, secure anchoring, and expanded indications for an aging population, the surface texture and morphology of dental and orthopedic titanium implants have not significantly improved over the last three decades since the advent of microrough surfaces in the early 90s [1–7]. Microrough surfaces have the advantages of increased bone-implant contact or osseointegration [4,8,9] and increased mechanical interlocking with bone compared with relatively smooth surfaces like machined surfaces [10–14]. The increased bone-implant contact is a consequence of rapid bone

* Corresponding author. Weintraub Center for Reconstructive Biotechnology and the Division of Regenerative and Reconstructive Sciences, UCLA School of Dentistry, 10833 Le Conte Avenue, Los Angeles, CA 90095, USA.

E-mail address: kkomatsu@g.ucla.edu (K. Komatsu).

https://doi.org/10.1016/j.mtbio.2023.100852
Received 25 May 2023; Received in revised form 21 October 2023; Accepted 29 October 2023
Available online 4 November 2023

formation, which minimizes soft tissue intervention [15–18]. Advantages of microrough surfaces also include harder and stiffer mineralized tissue formed on their surfaces than that on machined, smooth surfaces [17,19,20]. Stronger bonding is also established at the molecular level between bone and microrough surfaces [21–23]. However, there is less bone volume around microrough surfaces due to the inverse correlation between osteoblast proliferation and differentiation [24–27]. It is the biological principle that osteoblasts differentiate faster but proliferate slower on rougher surfaces [26,28–30].

Promoted differentiation of osteoblasts on microrough titanium surfaces has been demonstrated at the cellular phenotypic and molecular genetic levels. For instance, alkaline phosphatase activity, an early-stage biomarker of osteoblastic differentiation, as well as the amount of mineralized matrix deposition, a late biomarker, are increased on microrough surfaces [17,27,31]. At the genetic level, bone extracellular matrix (ECM) and growth factor genes are upregulated around microrough surfaces both *in vitro* and *in vivo* [18,30,32,33].

To further improve bone-and-implant integration or osseointegration, different surface modification techniques have been introduced. Adding surface topographies other than the micron level is effective. Titanium surfaces with micro-and-nano topography promotes osteoblastic differentiation over surfaces with micro-topography alone [34–37]. Physicochemical modification of titanium, such as the conversion to hydrophilic surfaces, increased bone-and-implant integration [38–42]. Variations in surface chemistry like a change in superficial oxide layer on titanium and the use of different titanium alloy also improve the osteogenic response [43–45]. Biological modification, such as coating titanium with proteins and other biological agents, positively affect osteoblastic differentiation [46–48]. Despite these successful efforts, most of the reported techniques remain at the experimental or developmental stage and not available clinically. More importantly, while there has been excellent descriptive evidence of accelerated osteoblastic differentiation and bone formation by the modified titanium surfaces, there is a significant knowledge gap about why the surface features influence osteoblastic differentiation, in particular, why increased surface topography triggers osteoblastic differentiation and, instead, delays osteoblastic proliferation.

Here we focused on the most representative surface topographical modification in dental and orthopedic implants, micro-roughening and attempted to identify a potentially distinct genetic profile responding to it. The objective of this study was to compare the transcriptional profiles of osteoblasts cultured on titanium surfaces with two different topographies: machine-smooth and acid-etched microrough titanium surfaces. We hypothesized that while the transcriptomes of osteoblasts grown on the two topographies would be largely similar, the transcriptomes would also reveal potential molecular mechanisms triggering accelerated osteoblastic differentiation and other distinct behaviors such as cell spreading and reduced proliferation on microrough surfaces. In doing so, we aimed to identify distinct groups of differentially expressed genes other than known bone-related marker genes that characterize the two topographies.

2. Material and methods

2.1. Characterization of titanium disk surfaces

Since osteoblasts react differently to different materials and surface topographies, it is critical to describe and characterize those features. Commercially pure grade 4 titanium disks (diameter 20 mm) were prepared either by machine-turning or acid etching with 67 % (w/w) sulfuric acid (H_2SO_4) at 120 °C for 75 s, following the protocol reported elsewhere [49,50]. The surface morphology of each of acid-etched and machine-smooth titanium disk was examined by scanning electron microscopy (SEM; XL30, Philips, Eindhoven, Netherlands) and laser profile microscopy (VK-8500, Keyence, Osaka, Japan) to quantify average roughness (Sa), peak-to-valley roughness (Sz), developed interfacial area ratio (Sdr), skewness (Sk), core void volume (Vvc), and kurtosis (Sku). These qualitative and quantitative surface analyses were based on the established characterization methods [29,30].

2.2. Bone marrow-derived osteoblast culture

Primary osteoblasts from rat bone marrow provide an *in vitro* culture model with excellent genetic stability and reliability of detecting expected cellular phenotypes [51,52]. Bone marrow-derived cells isolated from the femurs of 8-week-old male Sprague Dawley rats were cultured in alpha-modified Eagle's medium supplemented with 15 % fetal bovine serum, 50 μg/ml ascorbic acid, 10 mM Na-β-glycerophosphate, 10^{-8} M dexamethasone, and antibiotic–antimycotic solution containing 10,000 units/ml penicillin G sodium, 10,000 mg/ml streptomycin sulfate, and 25 mg/ml amphotericin B, following the previously established method [53,54]. Cells were incubated at 37 °C, 5 % CO_2 in a humidified incubator (ARC #2005-175-41 E, approved on January 30, 2018). Sub-confluent cells were detached by trypsin-EDTA and sub-cultured in new dishes. The culture medium was changed twice a week. Cells were seeded at a density of 2×10^4 cells/cm^2 on titanium disks in polystyrene 12-well culture dishes.

2.3. Osteoblast attachment and proliferation assays

Different biomaterial surfaces show different ability to recruit cells and allow them to proliferate. We therefore evaluated the number of cells attached during the initial stage of culture and cell density grown during the subsequent culture period using a previously reported method [55,56]. The number of osteoblasts attaching to titanium surfaces during the initial stage of cell culture was assessed using a tetrazolium salt (WST-1)-based colorimetric assay (Roche Applied Science, Mannheim, Germany) on day 1 of culture. Next, the density of propagated cells was quantified with the WST-1 assay on days 3 and 5. Additionally, to further understand the cell cycle progression, proliferative activity was assessed by BrdU incorporation (Roche Applied Science) during DNA synthesis on day 2. Osteoblasts on titanium were observed by fluorescence microscopy on days 1, 3, and 5 to verify their behavior. Cells were fixed in 10 % formalin and stained with the fluorescent dye rhodamine phalloidin (actin filaments, red; Molecular Probes, Eugene, OR, USA) and 4',6-diamidino-2-phenylindole (DAPI) (nuclei, blue; Abcam, Cambridge, UK). The expression levels of actin, the cell area, and perimeter were quantified using an image analyzer ImageJ (NIH, Bethesda, ML, USA).

2.4. Real-time quantitative polymerase chain reaction (qPCR)

Osteoblasts express different biomarker genes according to their differentiation stages. The expression of osteoblast-related genes was examined by qPCR at three different time points to identify the level of osteoblast differentiation. As described elsewhere [57], total RNA was extracted from cells using TRIzol (Invitrogen, Carlsbad, CA, USA) and a Direct-zol RNA MiniPrep kit (Zymo Research, Irvine, CA, USA) on days 5, 7, and 10. Extracted RNA was reverse transcribed into first-strand cDNA using SuperScript III Reverse Transcriptase (Invitrogen). Quantitative PCR was performed in a 20 μL volume containing 90 ng cDNA, 10 μL TaqMan Universal Master Mix II, and 1 μL TaqMan Gene Expression Assay using a QuantStudio 3 Real-Time PCR System (Thermo Fisher Scientific, Canoga Park, CA, USA) to quantify the expression of type I collagen, osteopontin, and osteocalcin mRNA. *Graph* expression was used as the endogenous control.

2.5. Alkaline phosphatase (ALP) activity

The ALP activity is a representative cellular phenotype during the early stage of osteoblastic differentiation. As reported previously [58,59], the cultured samples at day 5 were rinsed with double-distilled

water (ddH_2O) and treated with 250 μL *p*-nitrophenylphosphate (Wako Pure Chemicals, Richmond, VA, USA) and further incubated at 37 °C for 15 min. ALP activity was evaluated as the amount of nitrophenol released through the enzymatic reaction and measured at a wavelength of 405 nm using a microplate reader.

2.6. Alizarin red staining and quantitative analysis

Extracellular matrix mineralization is a final-step functional events representing osteoblastic differentiation. Alizarin red staining is a common way to detect the mineralized matrix. As reported elsewhere [60], after osteogenic induction for 5 and 14 days, samples were washed three times with PBS and fixed in 10 % formalin for 10 min before being stained with 1 % alizarin red solution (Sigma-Aldrich, St. Louis, MO, USA) for 5 min at room temperature. For the quantitative analysis, the dyed samples were dissolved in 10 % acetic acid for 30 min before adding 200 μl 10 % ammonium hydroxide to neutralize the acid. The optical density was measured at 405 nm using a microplate reader.

2.7. RNA sequencing (RNA-seq) and data analysis

As mentioned earlier, assessing the expression of particular genes will identify the functional/differentiation stage of cells. RNA-seq exploits the advantages of the next-generation sequencing and allows for a genome-wide large-scale gene expression profile. RNA-seq was performed on cells in the early stage of differentiation to understand the initial, overall molecular responses to surface topographies and identify a set of genetic factors that proceeds and triggers the subsequent promotion of osteoblastic differentiation. RNA was extracted from osteoblasts cultured for 5 days. The quality of extracted RNA was assessed with an Agilent 2200 TapeStation (Agilent Technologies, Santa Clara, CA, USA), and the resulting libraries were prepared using the Kapa mRNA HyperPrep Kit (Roche Diagnostics, Basal, Switzerland). These libraries were sequenced using single-end 50 bp reads on an Illumina HiSeq3000 sequencer (Illumina, San Diego, CA, USA) at the Technology Center for Genomics & Bioinformatics (TCGB) core at UCLA. Raw sequencing read data was verified and visualized with FastQC (v0.11.7). Subsequently, data were analyzed using the RaNA-Seq [61] cloud platform for FASTQ preprocessing (fastp 0.19.4) [62], which then aligned the data to the reference genome (Rnor_6.0). Samples were quantified (salmon 0.9.6) [63] to obtain read counts using the default parameters. The processed data were analyzed using integrated differential expression and pathway analysis (iDEP.96) [64]. In the iDEP package, read count data were normalized by counts per million in edgeR [65]. Additionally, genes with low expression levels (<1.0 counts per million [cpm]) were filtered from all downstream analyses, and only genes expressed in at least two samples were considered. Normalized count data were logarithmically transformed, ranked according to standard deviation across all samples, and the top 1000 genes were used in hierarchical clustering via the heatmap.2 function in the *gplots* package. Principal component analysis (PCA) was conducted using the transformed data, and differentially-expressed genes (DEGs) were detected using the *DESeq2* [66] package with a false discovery rate (FDR) < 0.01 and gene expression $|\text{fold change}| > 3.0$ as cut-offs. The detected DEGs were then visualized with volcano and MA plots, and gene lists were used for enrichment analysis using gene ontology (GO) terms. Additionally, detected DEGs were visualized using ShinyGO v.7.7 [67], sorted in descending order by fold enrichment within each pathway database, and represented through bubble plots. Pathway networks were created based on the number of genes shared between the nodes and the statistical value of gene set size. For analysis of Kyoto Encyclopedia of Genes and Genomes (KEGG) pathways, fold-changes of relevant genes were visualized in a pathway diagram using the Pathview Bioconductor package with a $|\text{fold change}| > 3.0$ threshold [68].

2.8. Immunofluorescence analysis

Immunofluorescence assays were performed to evaluate the expression of fibronectin, cyclin D1, and proliferating cell nuclear antigen (PCNA) in protein level. One day post-cultivation, the fixed cells were probed with primary antibodies specific for cyclin D1 (Invitrogen), PCNA (Invitrogen), and fibronectin (Proteintech, Rosemont, IL, USA). Detection was achieved using goat anti-mouse IgG FITC (Abcam) for cyclin D1 and fibronectin, while goat anti-rabbit IgG conjugated with cyanine5 (Invitrogen) was utilized for PCNA. Subsequent to antibody incubation, cellular morphology was visualized by staining F-actin with phalloidin, and nuclei were delineated using DAPI. The stained specimens were then visualized and captured with a fluorescence microscope. Protein expression levels were measured by calculating the mean gray value using ImageJ. The proportions of PCNA and cyclin D1-positive cells were determined by the percentage relative to the total cells within a site.

2.9. Collagen production

Collagen production was measured on day 5 by picrosirius red staining (Polysciences Inc., Warrington, PA, USA) Prior to staining, cells were washed with PBS and fixed in 10 % formaldehyde for 5 min. Subsequently, cells were stained with 0.1 % picrosirius red solution for 60 min at room temperature, after which 0.1 N sodium hydroxide was added for 60 min to elute the bound dye. The supernatant was measured at an absorbance of 550 nm using a microplate reader.

2.10. Cell cycle analysis

To validate the decrease in cell proliferation on microrough surfaces, we conducted a cell cycle analysis using Cell Cycle Assay Solution Blue (Dojindo Laboratories, Kumamoto, Japan). Briefly, osteoblasts cultured on both smooth and microrough surfaces were collected on day 5 and incubated with 5 μL of the assay solution at 37 °C for 15 min. The DNA content was subsequently determined using a Gallios flow cytometer (Beckman Coulter, Miami, FL, USA). Then, cell distribution in the G1, S, and G2 phases was analyzed, and the G2/G1 and S/G1 ratios were calculated.

2.11. Intracellular reactive oxygen species (ROS) and glutathione level

To detect intracellular ROS, cells were first washed with PBS. Subsequently, they were incubated in the dark with 5 μM CellROX Green reagent (Thermo Fisher Scientific) at 37 °C for 30 min. After incubation, the cells were fixed in 10 % formalin and stained with rhodamine phalloidin for actin filaments and DAPI for nuclei. Following thorough washing, the fluorescence levels within the cells were observed under a fluorescence microscope. The fluorescence intensity of ROS per cell was analyzed by imageJ.

For the quantification of total intracellular glutathione, a 5,50-dithiobis (2-nitrobenzoic acid) (DTNB)-based kit (Dojindo Laboratories) was used. Reduced glutathione (GSH) was masked using a specific reagent, allowing for the selective detection of oxidized glutathione (GSSG). Five days post-seeding on titanium disks, cells were lysed, and the supernatant was treated with DTNB and glutathione reductase at 37 °C for 10 min. Absorbance at 405 nm was used to determine both total glutathione and GSSG concentrations.

2.12. Statistical analysis

Surface roughness parameters were measured from five different locations on multiple disks ($n = 5$). Three disks were used for cell culture studies and RNA-seq ($n = 3$). Ten different sites were quantified in the fluorescence microscopy analysis ($n = 10$). Statistical analyses were performed using GraphPad Prism 9.0 software (GraphPad, Chicago, IL,

USA). Two-way ANOVA was used to examine the effect of titanium surface and days in culture on both qPCR and the quantification of alizarin red staining. When necessary, a Bonferroni test was used as a multiple-comparison test. The unpaired *t*-test was used to determine differences between two groups. A p-value less than 0.05 was considered statistically significant. DEGs were identified based on a q-value <0.01 and fold-change of normalized counts ≥ 3.0.

3. Results

3.1. Surface characterization of titanium samples

SEM images of the machine-turned titanium disks showed no definable topography except for line traces, burrs, and irregularities from machine turning (Fig. 1A). Acid-etched disks showed compartmental structures all over the surface consisting of peaks and valleys of 1–5 μm pitch. Quantitative roughness analysis revealed that the Sa, Sz, Sk, Vvc, and Sku were 2–4 times greater for the acid-etched surface than the machine-turned surface (Fig. 1B). Sdr was 8-times higher for the acid-etched surface. Due to the small and large vertical deviations of the two surfaces, respectively, machine-turned surfaces are termed a "smooth" surface, while the acid-etched surface is a "microrough" surface in this study.

3.2. Osteoblastic phenotypes on different surface topographies

We first verified our *in vitro* osteoblastic culture system by determining whether osteoblasts showed characteristic phenotypes on smooth and microrough surfaces. More osteoblasts attached to smooth surfaces than microrough surfaces after one day of culture (Fig. 2A and B). The number of cells proliferating during subsequent culture over 3 and 5 days was also greater on smooth surfaces (Fig. 2C and D), as confirmed by BrdU incorporation (Fig. 2E). Gene expression of bone-related extracellular matrix markers, i.e., collagen type 1, osteopontin, and osteocalcin, was upregulated on microrough surfaces on day 10 but not significantly so on day 5 (Fig. 2F). ALP activity was significantly higher on microrough surfaces at day 5 (Fig. 2G). However, we detected the minimal mineralized matrix at this time point, indicating that mineralization did not occur yet (Fig. 2H). By day 14, the quantity of mineralized matrix significantly increased on microrough surfaces, demonstrating the progression of osteoblast differentiation and mineralization.

3.3. General comparison of transcriptional profiles between the two surface topographies

We next compared the transcriptional profiles of osteoblasts grown on smooth and microrough surfaces during early-stage culture (day 5) by RNA-seq analysis. As shown in the representative EdgeR scatter plots comparing cells grown on the same surfaces (Fig. 3A and B), gene expression was very highly correlated in cells grown on the same topography ($r = 0.994$ for the smooth group; $r = 0.992$ for the microrough group). Although still high, correlation was lower between the smooth and microrough surfaces ($r = 0.975$) than within the same surface group (Fig. 3C). The results of regression analysis were summarized in a correlation heat map (Fig. 3D), which clearly illustrated the very high intra-topography correlation (dark blue to blue in Fig. 3D) and the high inter-topography correlation (white to light blue) of the transcriptional profiles, with an appreciable difference for the two correlations. PCA showed that the genes from the two different topographies were well separated along PC1, indicating distinct gene profiles (Fig. 3E). Finally, hierarchical clustering of the top 1000 differentially expressed genes across surface types and samples clearly showed transcriptional cohesion within the same topography and clear distinction of clusters between topographies (Fig. 3F), re-confirming the transcriptional similarity within the same topography group but differences between the different topography groups. Several gene clusters showed clear, cohesive differential expression (i.e., either upregulated or downregulated for each topography group), while other gene clusters were mixed. Together, these indicate the uniformity of the experimental RNA samples and persistent transcriptional differences according to surface topography.

3.4. Differentially-expressed genes (DEGs) between two different surface topographies

We next identified DEGs between smooth and microrough surfaces. Out of 13,049 quality-filtered genes, 229 (1.75 %) were differentially expressed according to criteria of $|\text{fold change}| > 3.0$ and $q < 0.01$, of which 180 genes (1.38 %) were upregulated in cells grown on microrough surfaces and 49 (0.37 %) were downregulated (Fig. 4A and Table S1). The DEGs were then visualized in a 2D volcano plot in terms of fold-change (X-axis) and statistical significance (Y-axis) (Fig. 4B) and as MA plots in terms of the expression levels for each of the smooth (Y-axis) and microrough (X-axis) surfaces (Fig. 4C).

GO enrichment analysis revealed that the pathways upregulated on microrough surfaces containing the highest number of DEGs were the immune system process (72 genes) in the biological process category, plasma membrane (60 genes) in the cellular component category, and molecular function regulator (28 genes) in the molecular function category (Fig. 4D and Tables S2–4). On the other hand, the pathways showing the highest fold enrichment were leukocyte migration in the biological process category, filopodium in the cellular component category, and chemokine activity in the molecular function category. In the KEGG pathway analysis, *Staphylococcus aureus* infection was observed to have the highest fold enrichment, followed by viral protein interaction with cytokine and cytokine receptor (Fig. 4D and Table S5). A majority of DEGs downregulated on microrough surfaces were in the cellular component category (Table S6).

We then visualized the interaction networks of the pathways (Fig. 4E). First, all functional nodes/pathways were large and extensively interconnected in the biological process category, with core pathways of the immune system process, immune response, regulation of immune system processes, and responses to external stimuli. Second, in the cellular component category, node connections were found between the plasma membrane and integral component of plasma membrane and between the cell surface and the external side of plasma membrane. In the molecular function analysis, a wide network was centralized with signaling receptor binding as a core node. Also, signaling receptor activity, transmembrane signaling receptor activity, and molecular transducer activity were strongly connected.

In the process of osseointegration, cell adhesion, signaling, and interactions with the ECM are crucial. Hence, we undertook four target-specific KEGG enriched pathway analyses (Fig. 5). The analyses in the tight junction and adherence junction revealed upregulation of Rho family G-protein signaling pathways (Rac, CDC42, WASP) and actin-related genes (*actin*, *arp2/3*) on microrough surfaces (Fig. 5A, B). In the tight junctions, we also found stress-induced upregulation of *CaV1.3* and *Contactin*. Of note, claudin, a key trigger of the tight junction cascade, was downregulated on microrough surfaces. Furthermore, co-upregulation of *PCNA* and *cyclin D1* was detected. In the analysis of ECM-receptor interactions, there was extensive microrough surface-induced upregulation of ECM genes such as laminin, fibronectin, and collagen and the integrin alpha subunit families (Fig. 5C). The ECM-membrane glycoprotein/proteoglycan interaction was also upregulated, among which, laminin, fibronectin, CD36, and thrombospondin are disulfide-linked or -targeted ECM or membranous glycoproteins. Similarly, the focal adhesion pathway showed high expression of integrin alpha subunit and focal adhesion-related signaling proteins like protein kinase C (PKC), Parvin, PI3K, myosin light chain kinase (MLC), and Vav on microrough surfaces, leading to upregulation of actin (Fig. 5D).

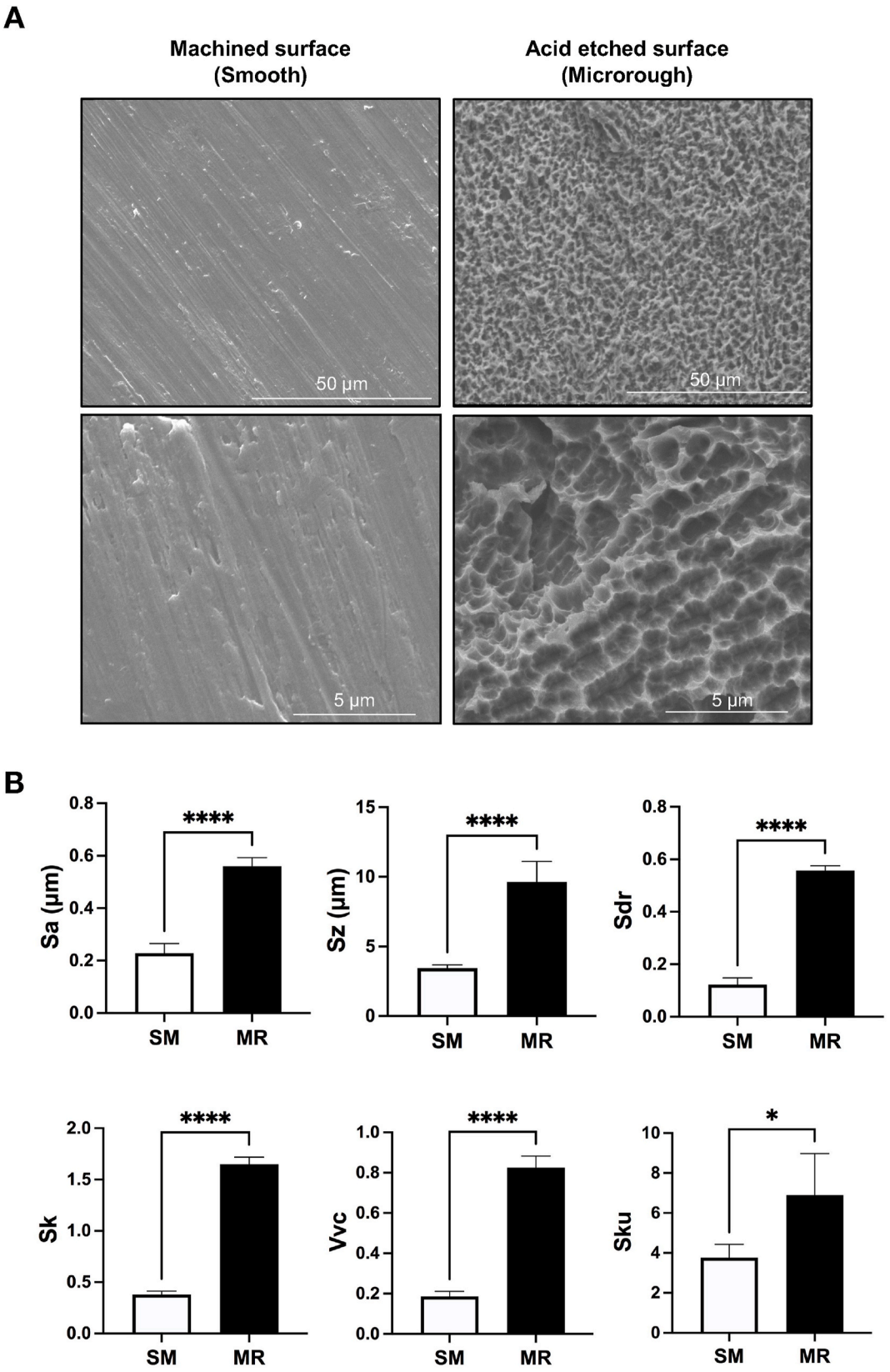

Fig. 1. Surface topography of titanium disks. (A) Scanning electron microscopy images of smooth (SM) and microrough (MR) titanium. (B) Quantification of surface roughness. The average roughness (Sa), peak-to-valley roughness (Sz), developed interfacial area ratio (Sdr), skewness (Sk), core void volume (Vvc), and kurtosis (Sku) are indicated. Each value represents the mean ± SD (n = 5).

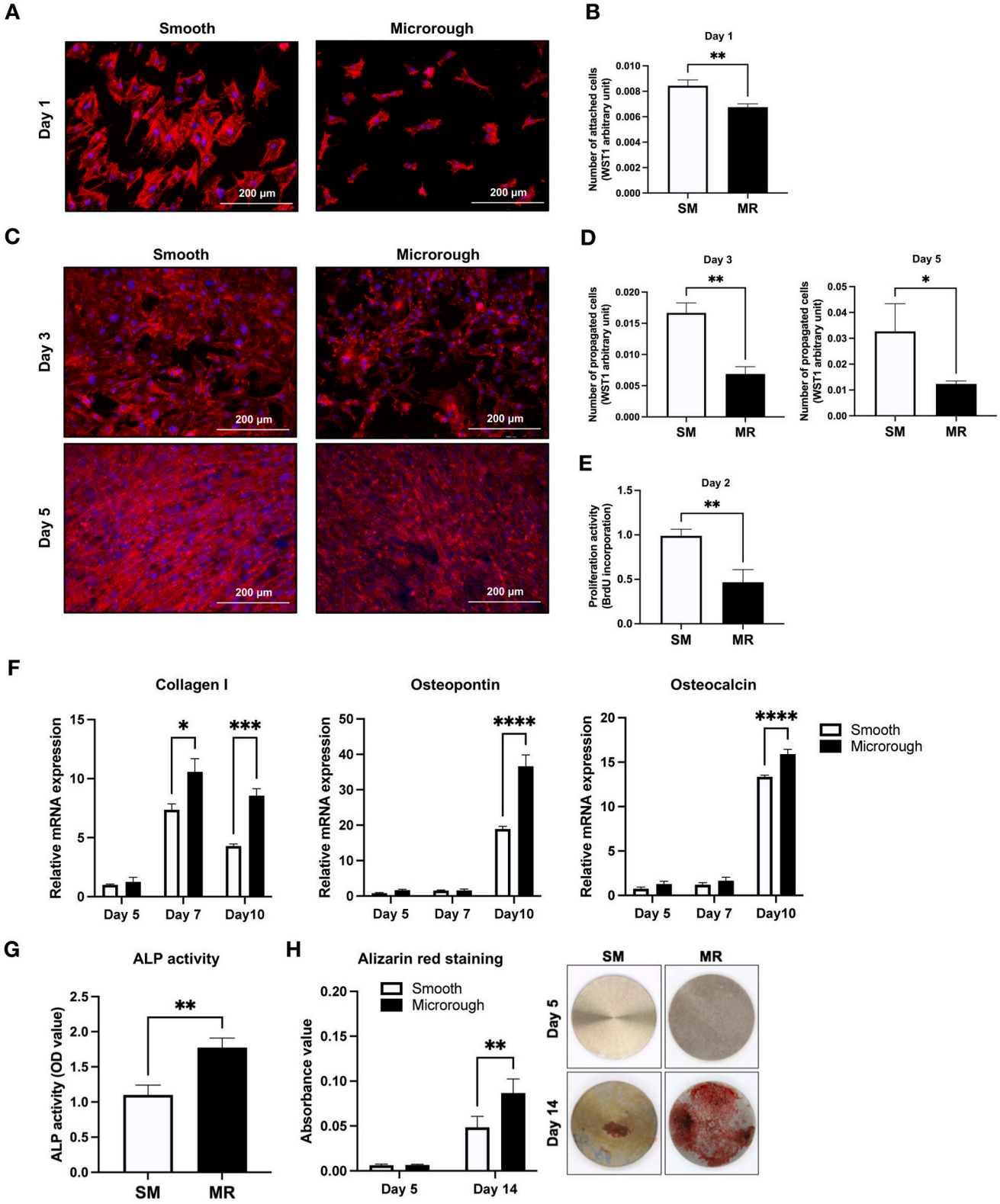

Fig. 2. Function and behavior of osteoblasts responding to different surface topographies. (A) Fluorescence microscopy images of osteoblasts on culture day 1 stained for cytoskeletal actin filaments and nuclei. (B) The number of cells attaching after one day of incubation evaluated by the WST-1 assay. (C) Fluorescence microscopy images of osteoblasts on culture days 3 and 5. (D) The number of proliferated cells on culture days 3 and 5 evaluated by a WST-1 assay. (E) Cell proliferation of osteoblasts evaluated by the BrdU assay on culture day 2. (F) Real-time qPCR analysis of mRNA expression of bone-related collagen type I alpha 1, osteopontin, and osteocalcin genes on days 5, 7, and 10. (G) Alkaline phosphatase (ALP) activity on day 5. (H) Matrix mineralization quantified by measuring alizarin red staining of the absorbance at days 5 and 14. Representative images of alizarin red staining on cultured smooth (SM, left) and microrough (MR. right) surfaces. All quantitative data are presented as mean ± SD (n = 3). *P < 0.05. **P < 0.005. ***P < 0.0005, ****P < 0.0001.

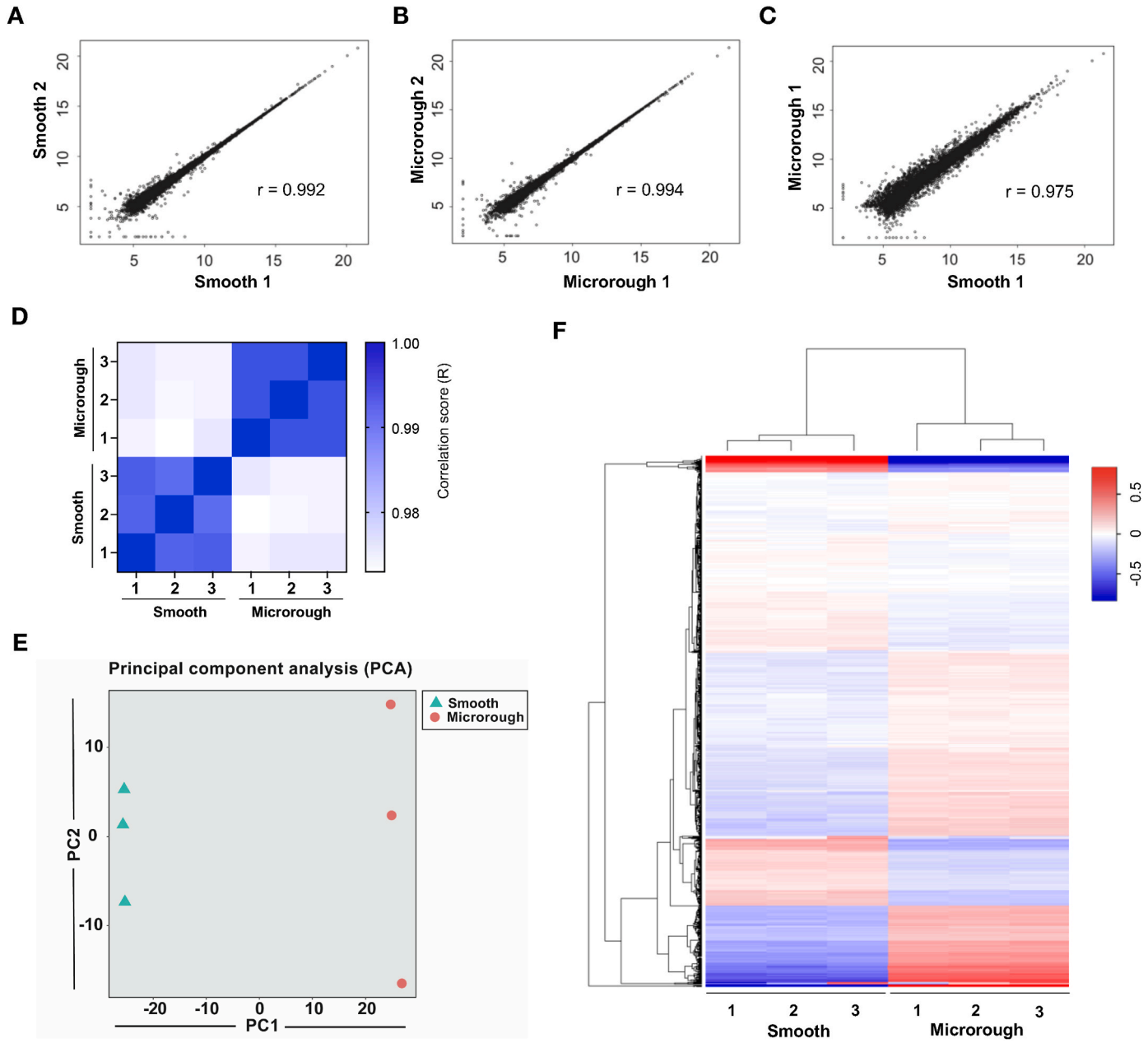

Fig. 3. General comparison of the transcriptional of smooth (SM) and microrough (MR) surfaces. Representative scatter plot of gene expression in the two samples, (A) smooth vs smooth, (B) microrough vs microrough, (C) smooth vs microrough. Each dot constitutes a gene. (D) Heatmap analysis based on correlation coefficients in scatter plots. (E) Gene expression patterns by principal component analysis. (F) Hierarchical clustering was used to evaluate the top 1000 genes with significant differential expression in the smooth and microrough groups. Each column represents one sample's expression pattern. The red lines represent upregulated genes and the blue lines represent the downregulated genes.

3.5. Actin expression and cytomorphologic modulation on microrough surfaces

To validate the findings from the KEGG pathway analysis at the protein level, we examined the expression and organization of the cytoskeletal protein, actin, using fluorescent staining at 24 h post-seeding (Fig. 6A). Actin expression per cell was significantly increased on microrough surfaces (Fig. 6B). Conversely, osteoblasts exhibited significant spreading on smooth surfaces, presenting a larger cell area compared to those on microrough surfaces (Fig. 6C). While there was no clear difference in cell perimeter between the two topographies, the perimeter/area ratio was markedly higher on microrough surfaces, indicating that osteoblasts on microrough surfaces exhibit a more complex morphology with an increased number of cell projections.

3.6. Enhanced ECM production on microrough surfaces

We next confirmed the upregulated expression of a representative ECM glycoprotein gene, fibronectin, at the protein level. An immunofluorescence analysis revealed a more than 25 % upregulation of fibronectin per cell on microrough surfaces (Fig. 7A and B). Given that the KEGG pathway analysis indicated an upregulation of collagen, a quantitative analysis utilizing sirius red staining was also conducted. The amount of collagen deposited on the microrough surfaces was significantly greater than on smooth surfaces on day 5 (Fig. 7C). These protein level evaluations were in agreement with the results from the KEGG pathway analysis, specifically within the ECM-receptor interaction pathway.

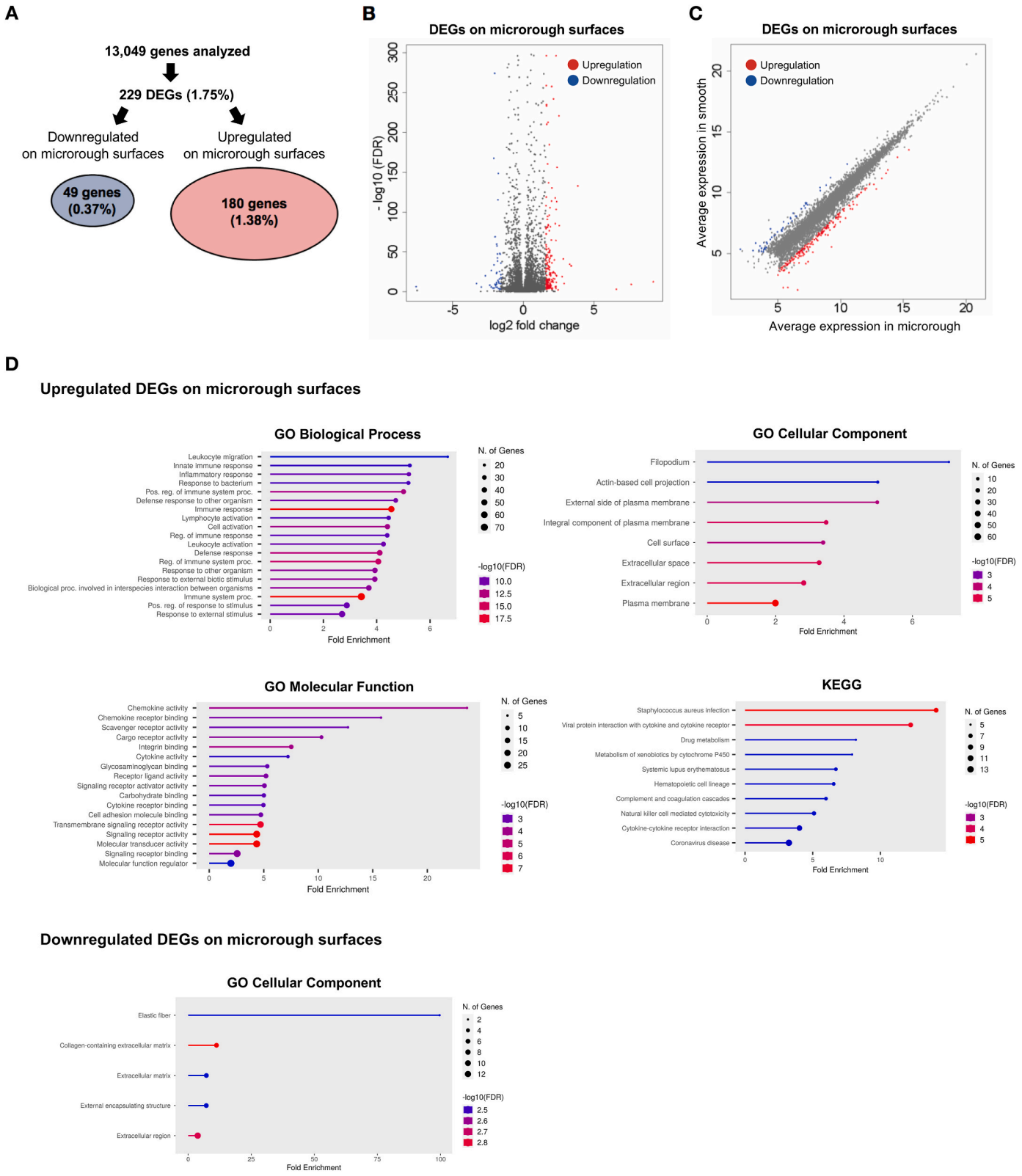

Fig. 4. Characterization of DEGs on microrough surfaces. (A) Summary of the total number of detected genes and DEGs both upregulated and downregulated (|fold change| > 3.0; q < 0.01). (B) Volcano plot and (C) MA plot of the DEGs between groups (red: upregulated genes; blue: downregulated genes). (D) Upregulated and downregulated DEGs on Gene Ontology (GO) and Kyoto Encyclopedia of Genes and Genomes (KEGG) pathway enrichment analyses. (E) Network of upregulated and downregulated genes on microrough surfaces. Pathways were connected if they shared >30 % genes. Green and red represent down- and upregulated pathways, respectively. Darker nodes were more significantly enriched gene sets, and bigger nodes represented larger gene sets. Thicker edges represented more overlapped genes.

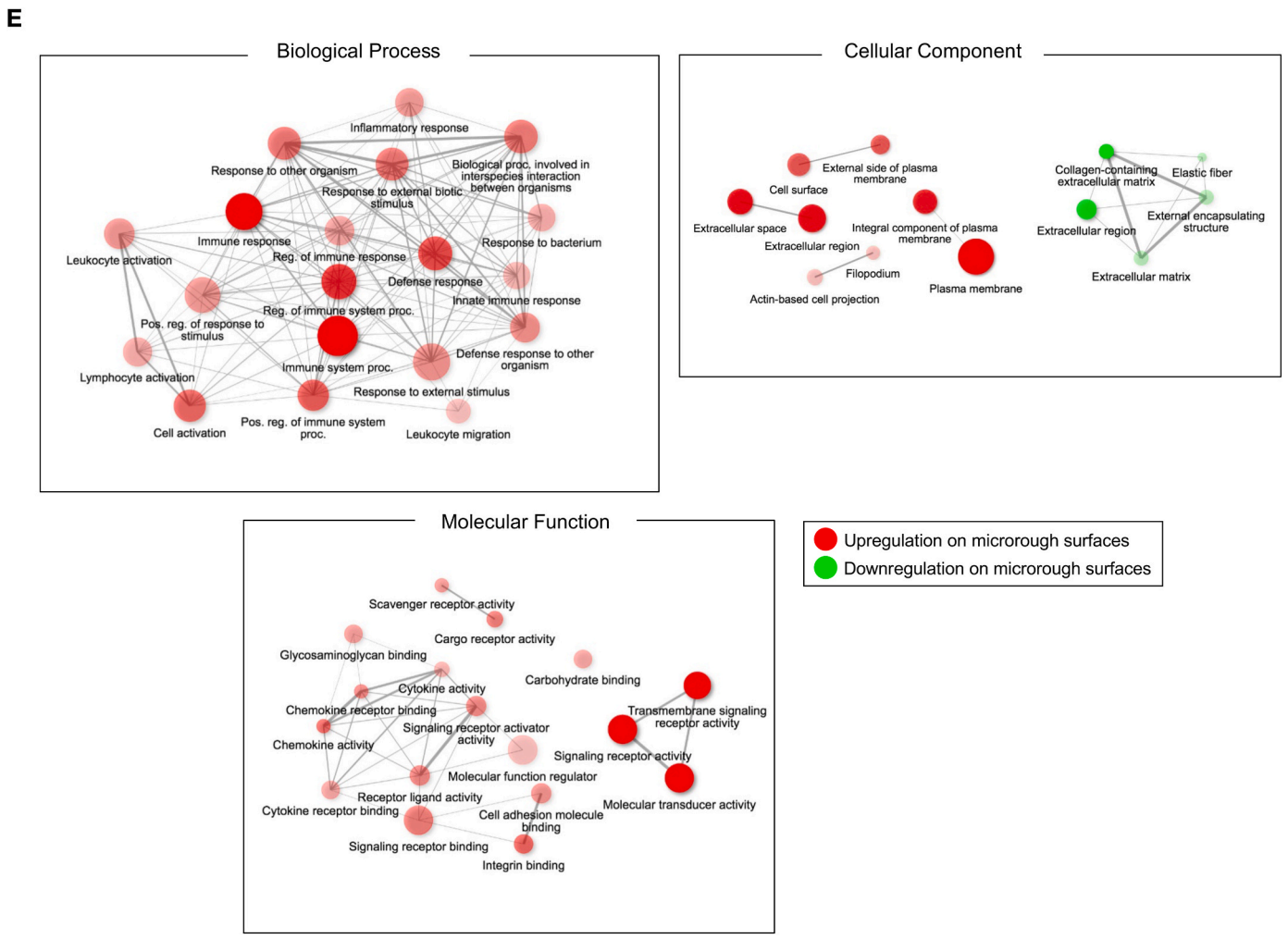

Fig. 4. (*continued*).

3.7. Reduced cell proliferation through co-expression of PCNA and cyclin D1 on microrough surfaces

To further analyze the reduced proliferation on microrough surfaces, we first assessed the co-expression of PCNA and cyclin D1 proteins after 24 h of cultivation. Although both surfaces displayed equivalent proportions of PCNA-positive cells, more cells were cyclin D1-positive on microrough surfaces, resulting in the higher percentage of cells that were positive both for PCNA and cycline D1 (Fig. 8A, B, C). To further substantiate these observations, we conducted cell cycle characterization via flow cytometry on day 5. While there were no significant differences in the proportions of cells in the G1 and G2 phases between the two surfaces, cells on microrough surfaces exhibited a smaller percentage of S phase and thereby a lower S/G1 ratio, revealing the specific modulation in cell proliferation in response to the microrough surface (Fig. 8D and E).

3.8. Osteoblast stress responses on smooth and microrough surfaces

The intracellular ROS level have a significant role in cellular signal transduction and the regulation of immune responses. Therefore, we examined the level of intercellular ROS production and glutathione level as an antioxidative response. Cells on microrough surfaces exhibited an increased ROS level compared with those on smooth surfaces after 24 h of culture (Fig. 9A and B). While there was no significant difference in the GSH levels between the two groups (Fig. 9C), cells grown on microrough surfaces exhibited a higher level of GSSG than those on smooth surfaces. Accordingly, GSSG/GSH was significantly higher on microrough surfaces, indicating the augmented stress response by the osteoblasts.

4. Discussion

Surface and intrinsic properties of biomaterials play a pivotal role in determining cellular fate and function [69]. Substrate stiffness, stress relaxation, and adhesion ligand density collectively influence cellular transcriptome and phenotype, as demonstrated in recent studies [70,71]. Nonetheless, previous studies examining cellular responses to titanium surfaces have been limited by their focus on specific candidate osteogenic, cell adhesion, and mineralization biomarkers [72–76]. Thus, although several studies have utilized microarray analyses to assess transcriptomes on materials with various surface topographies, they have not elucidated the core mechanisms responsible for observed benefits and/or suspected drawbacks [77–79]. Moreover, the emphasis in much of those studies has predominantly been on the development of novel materials with biological modification, such as coating with proteins and other biological agents, thereby overshadowing a comprehensive understanding of foundational osteoblast dynamics [80,81]. As a result, while it is generally accepted that microrough surfaces promote early osteoblast differentiation, the subtle shifts in transcription during these initial stages on currently used materials are yet to be fully deciphered. Further, a majority of papers studying osteoblasts on biomaterials have focused on how they can promote their differentiation and the reduced proliferation of osteoblasts on rough materials has

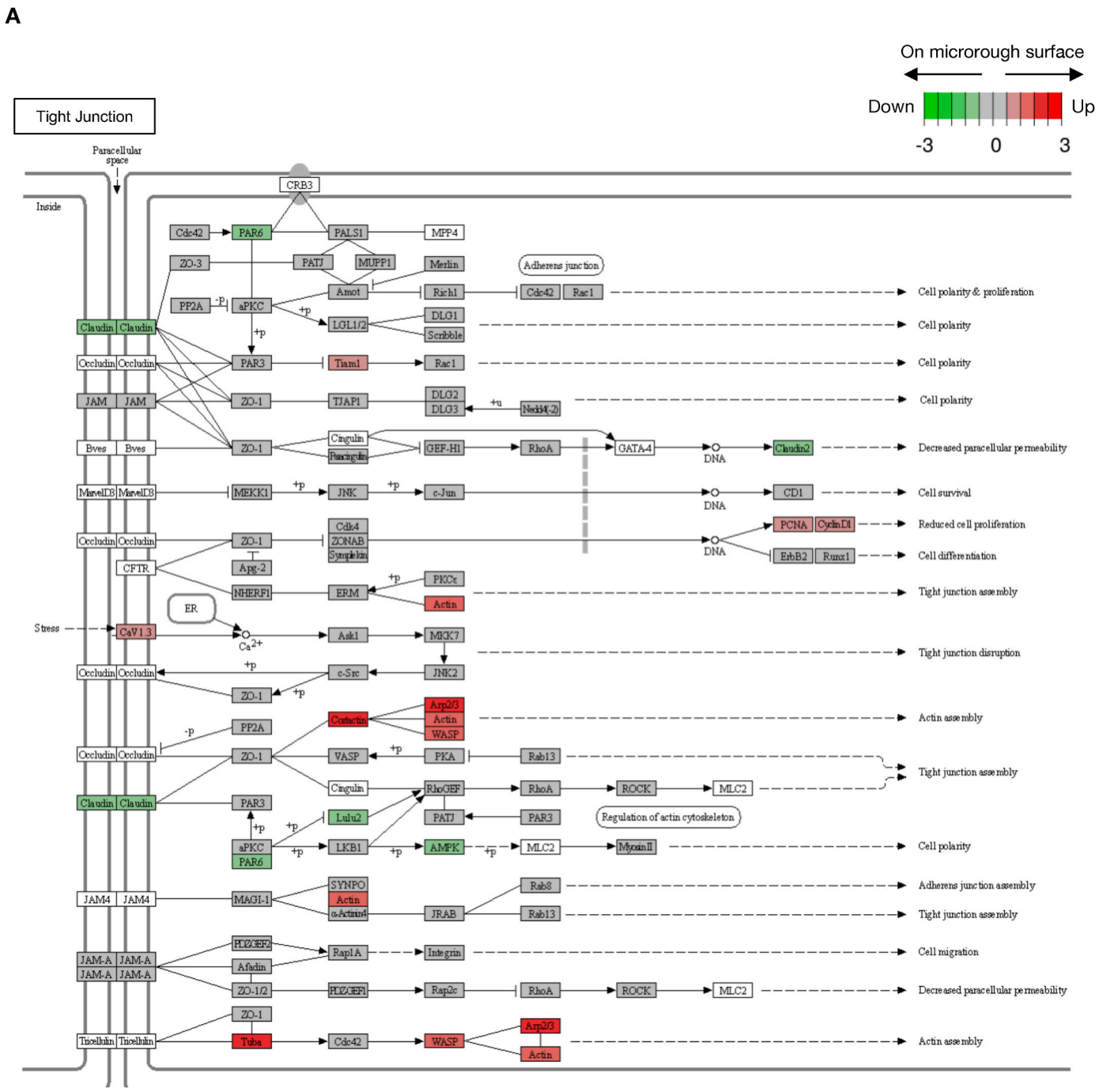

Fig. 5. Visualization of KEGG pathways. (A) Tight junction, (B) adherens junction, (C) ECM-receptor interactions, and (D) focal adhesion. Red denotes upregulated genes, green denotes downregulated genes.

rarely been addressed. Bridging these knowledge gaps is not only vital for a deeper insight into cell-biomaterial interactions but also crucial for advancing implant surfaces and pursuing other applications of titanium in the field of regenerative medicine. In this study, we uniquely mapped a comprehensive transcriptome profile of cellular responses to microrough titanium surfaces by RNA-seq. Given its broader dynamic range and superior detection capability [82,83], we favored high-throughput RNA-seq over microarrays, which is optimally suited for unraveling complex biological mechanisms [84]. Our study adopted an approach by integrating pathway, network, and KEGG analyses based on transcriptional profiles to build upon the foundational understanding of cell-biomaterial interactions. Although this approach is a staple in pathophysiological and pharmacological research [85,86], its application to the fields of biomaterials and implantology represents a novel and pioneering direction.

We began by validating our *in vitro* osteoblastic culture system, observing behaviors and responses of osteoblasts on different surface textures. Consistent with prior research, osteoblasts exhibited reduced attachment and proliferation but increased differentiation on microrough surfaces compared to smoother ones. Analysis of RNA-seq data by PCA and hierarchical clustering revealed that the transcriptional profiles of osteoblasts on microrough surfaces were fundamentally different to

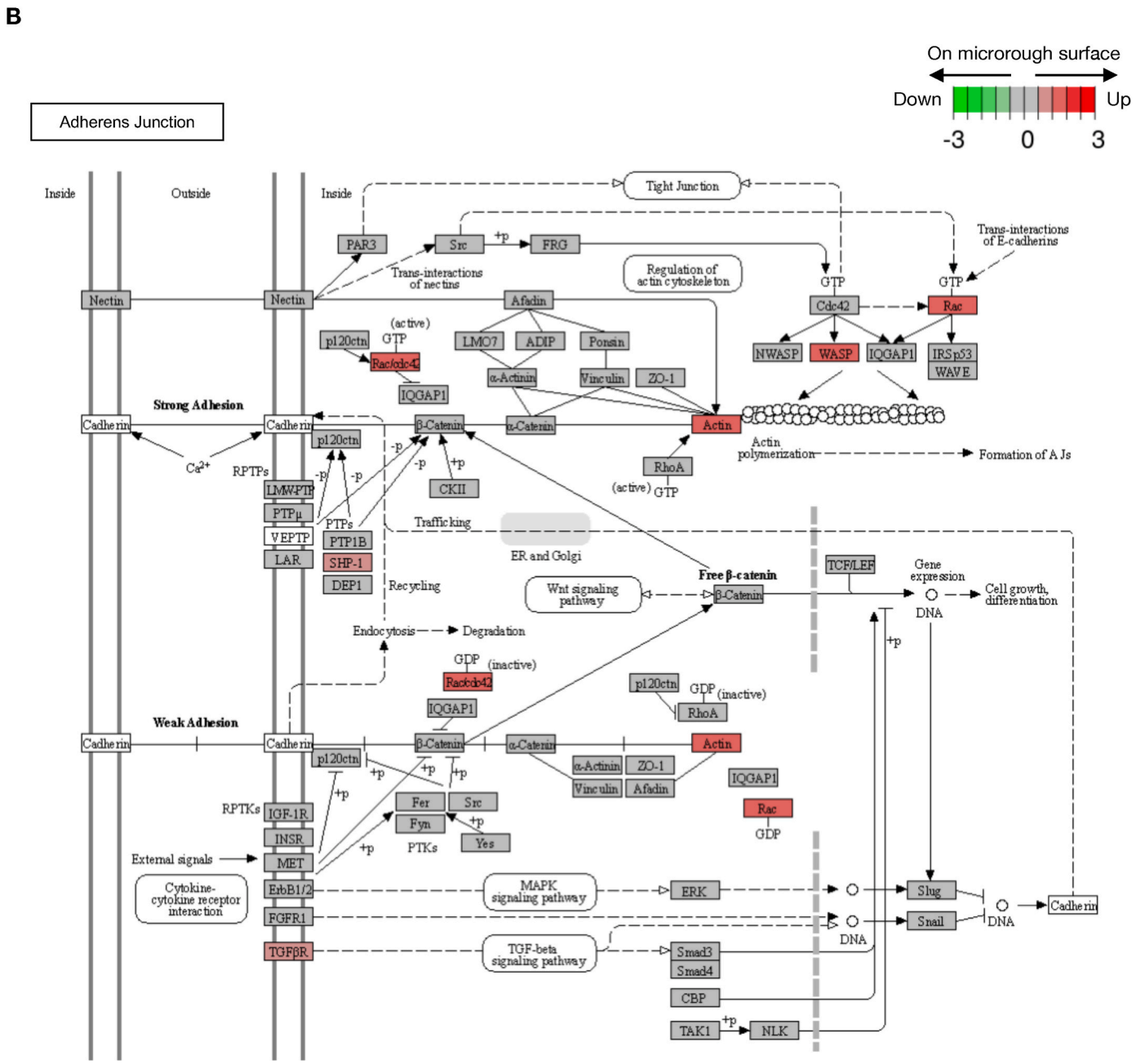

Fig. 5. (*continued*).

those on smooth surfaces. Within-group gene expression was consistent on both surfaces, validating the uniformity of our titanium disk models. Studies showed that osteoconductivity is higher with random and disorganized textures than with uniform and organized ones [87–89]. The widely-adopted acid-etched microrough surface in titanium implants [1,2] exemplifies this phenomenon. The present study demonstrated that stable transcriptional profiles can be obtained from RNA samples extracted from such random surface texturing.

Differential expression analysis revealed that 1.75 % of the total number of genes were DEGs, with 1.38 % upregulated and 0.37 % downregulated on microrough surfaces, highlighting that rough topographies favor transcriptional upregulation rather than downregulation. While limited data exists on DEGs related to biomaterial surfaces, a study investigating the effect of gel elasticity on epidermal ovarian cancer cells reported a 1.27 % change in gene expression relative to the control group; although this was a different cell type [90]. In the context of titanium implants, a microarray study revealed 31 out of 20,000 genes (0.016 %) were upregulated during bone healing [79], and another *in vivo* study found 3 upregulated genes out of 1900 around microrough implants using differential display PCR [91]. We detected a higher rate of differential expression in response to the two different surface topographies of titanium using RNA-seq.

We found that there was enrichment of upregulated genes related to responses to external stimuli and immune response pathways in osteoblasts grown on microrough surfaces, with network analysis highlighting these pathways as distinct features of these surfaces. Interestingly, KEGG pathway analysis showed an enrichment of pathways related to *Staphylococcus aureus* infection and viral protein interactions with cytokines, even in the absence of infectious agents in our controlled culture environment. This suggests the surface topography may mechanically stimulate the cells, triggering a cellular stress response resemblant to the defense mechanisms against infections.

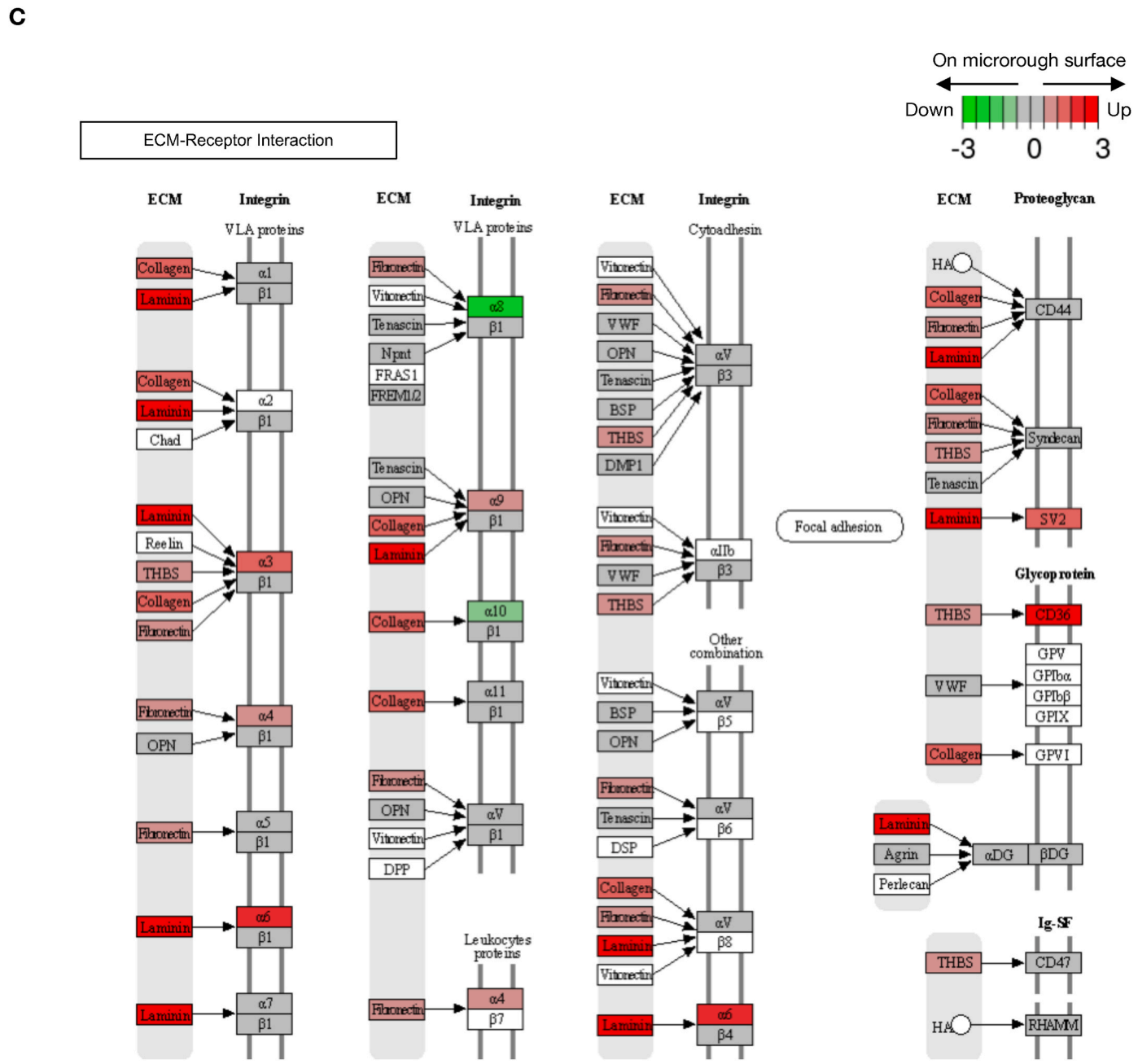

Fig. 5. (*continued*).

Supporting this notion, it is reported that bacterial infection responses and cellular stress responses often have overlapping gene expression patterns [92]. Previous studies have reported that cells cultured on biomaterial with different surface properties show the differential expression of oxidative stress markers [93,94]. Another study demonstrated that osteoblasts grown on microrough surfaces exhibit an enhanced response to mechanical stimulation [95]. Although these studies have provided valuable insights, comprehensive analyses of the stress and response mechanisms induced by the roughness of titanium surfaces at the cellular level have not been undertaken. Specifically, the nuanced interplay between mechanical stressors, intracellular ROS levels, and the consequent modulation of cellular and genomic responses has remained largely unexplored. Intracellular ROS, acting as secondary messengers in pathways, not only play a pivotal role in cellular signaling, but also in modulating immune responses by affecting cytokine production and inflammatory reactions. These reports and our data substantiate our hypothesis the mechanical stimulation from the microrough surface might elevate intracellular ROS levels, potentially amplifying cellular signaling and immune responses at the genomic level. Furthermore, the present study revealed the upregulation of cytokines and chemokines, as well as receptors essential for their signaling. It is well-established that cytokines are known to play a crucial role in osteogenesis [96], and chemokines and their receptors have been reported to be important in the differentiation of osteoblasts from osteoblast progenitor cells [97–99]. The present results on the upregulation of cytokines in osteoblasts on rough surfaces corroborated the previous studies [100,101].

Cells have the ability to perceive mechanical stimuli by transforming them into biochemical signals. In this process, actin, a prominent cytoskeletal protein, operates as a mechanosensor, detecting and responding to external stimuli [102–104]. Our results showed that cytoskeletal actin levels are higher both in transcriptional and protein levels on

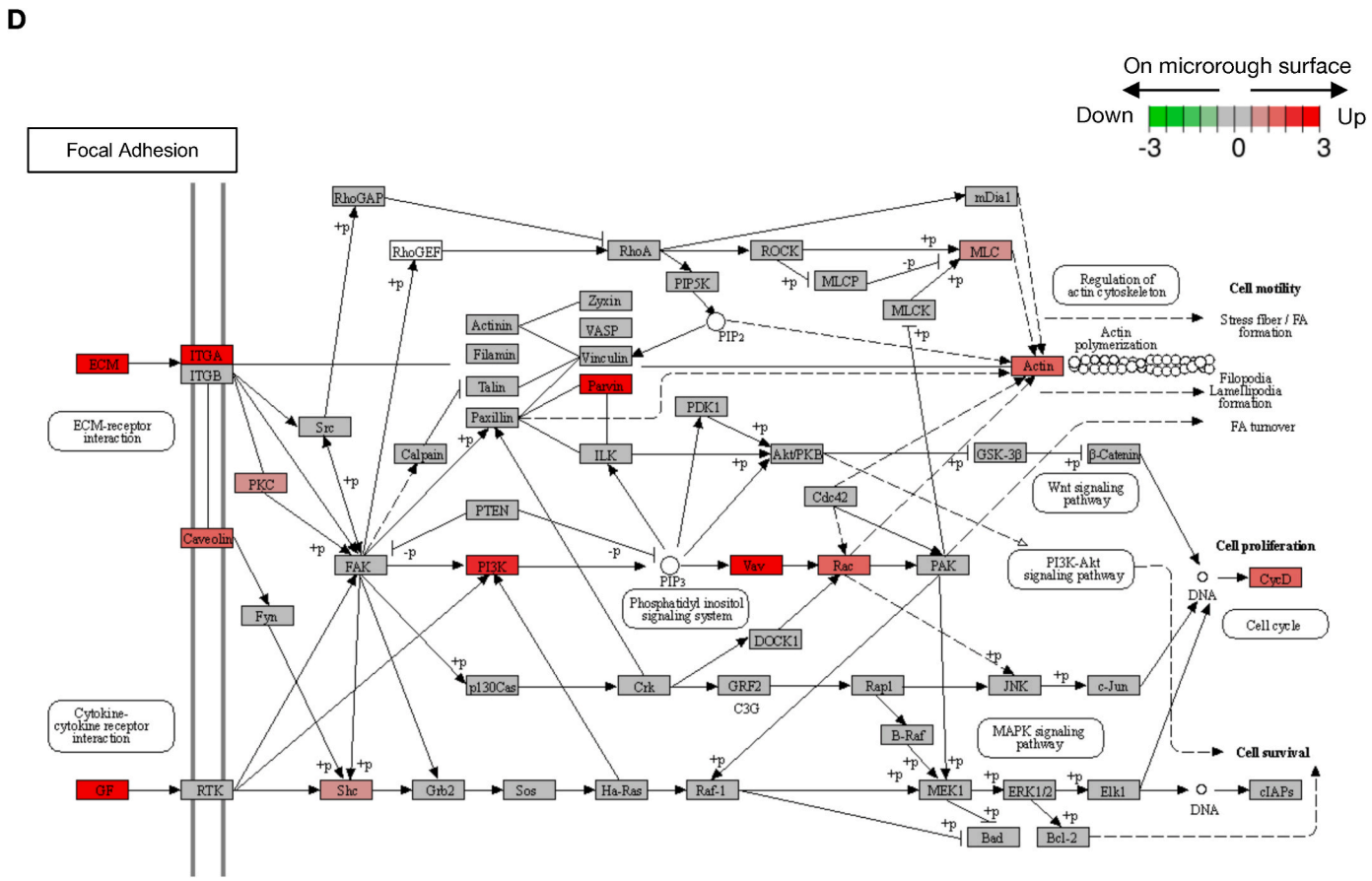

Fig. 5. (*continued*).

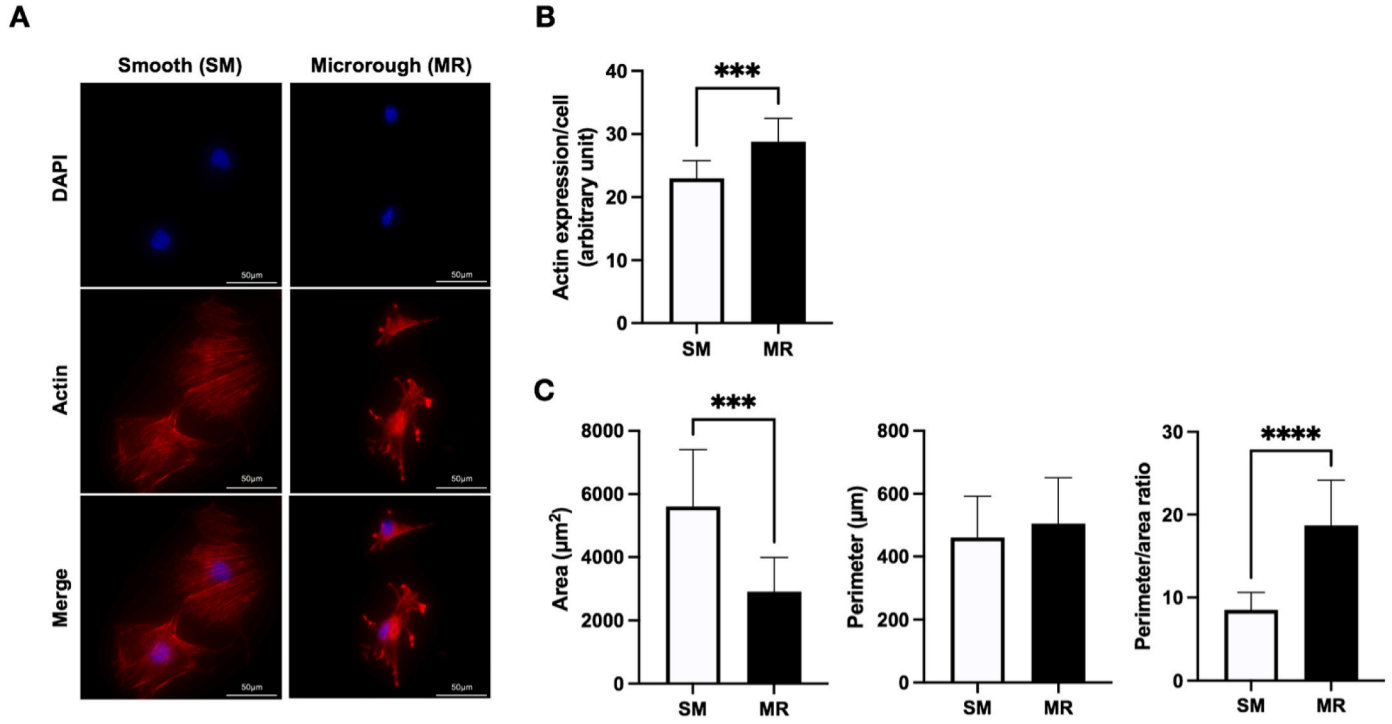

Fig. 6. Actin expression and cytomorphologic modulation of osteoblasts on different surface topographies after 24 h of culture. (A) Representative fluorescence microscopy images of osteoblasts on smooth and microrough surfaces. (B) Quantitative analysis of actin expression per cell. (C) Cytomorphometric analysis of osteoblasts showing cell area, perimeter, and perimeter/area ratio. All quantitative data are presented as mean ± SD (n = 10). ***P < 0.0005, ****P < 0.0001.

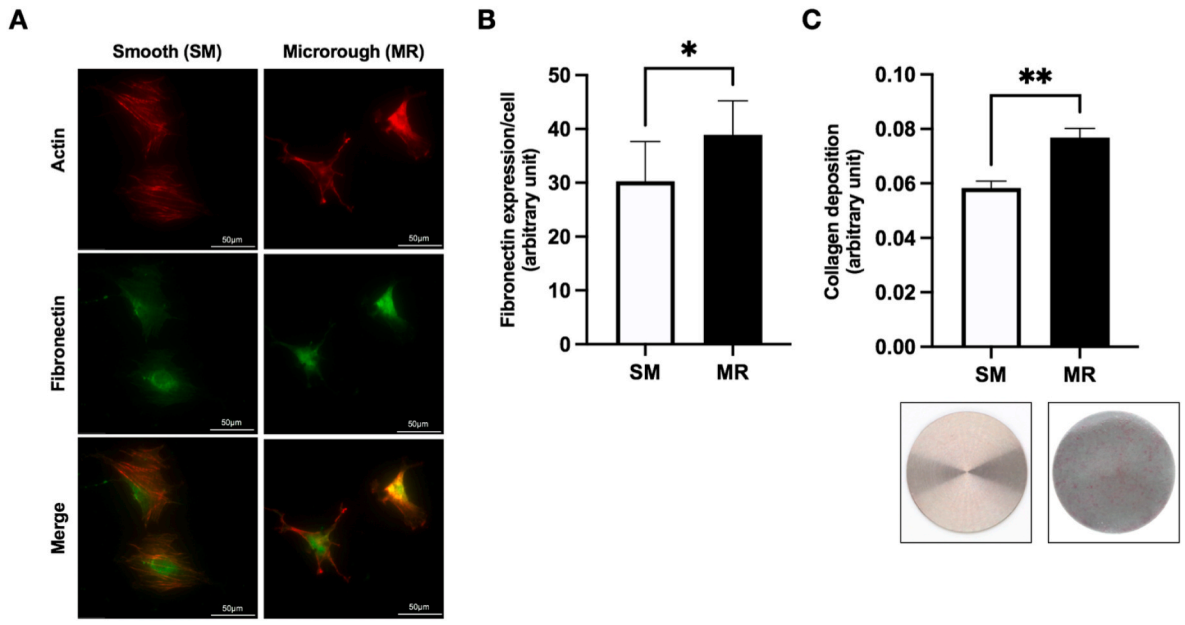

Fig. 7. Fibronectin expression and collagen deposition on different surface topographies. (A) Representative immunofluorescence images showing fibronectin expression of osteoblasts on smooth and microrough surfaces after 24 h of culture. (B) Quantitative analysis of fibronectin expression per cell. Data are presented as mean ± SD (n = 10). (C) Quantitative evaluation of collagen deposited on smooth and microrough surfaces on day 5. Data are presented as mean ± SD (n = 3). *P < 0.05, **P < 0.005.

microrough surfaces compared to smooth surfaces. Concurrently, we observed an increase in pathways related to filopodia and actin-based structures on these rougher surfaces. This upregulation in specific pathways resonates with the observed intricate morphology of cells on microrough surfaces, reinforcing the interplay between surface topography and cellular responses. This theory gains traction when considering the selective activation of the Rho family G-protein signaling pathway on these surfaces, a critical facilitator of actin filament assembly. Thus, the present results suggest that signal transduction pathways are strongly induced in cells growing on microrough surfaces, leading to changes in cytoskeleton and the formation of stress fibers and cytoplasmic projections in these cells. Additionally, it is interesting to note that claudin gene expression was downregulated in the tight junction analysis, perhaps due to weak cell-cell adhesion due to the lower number of cells on microrough surfaces. More importantly, intracellular signaling pathways were upregulated on microrough surfaces, even without the help of core genes triggered by cell-cell interactions such as claudin and occludin within the paracellular space.

Osteoblasts growing on rough surfaces exhibit a low capacity for proliferation compared with those grown on smooth surfaces, although the reasons for this remain uncertain [105,106]. We identified PCNA and cyclin D1 co-upregulated on microrough surfaces, consistent with cell cycle arrest and inhibition of proliferation. PCNA is an essential protein required for DNA replication [107–109], while cyclin D1 is a protein induced in the G1 phase of the cell cycle that undergoes activation through phosphorylation to progress the cell cycle [110,111]. However, co-expression of these proteins impedes DNA replication, halting cell cycle progression and proliferation [112]. Specifically, it was suggested that during the S phase, cyclin D1 can bind to PCNA, a critical regulator of DNA synthesis, thereby inhibiting DNA synthesis [113,114]. Further, cyclin D1 overexpression may result in the inhibition of DNA synthesis [112]. Our cell cycle assessment indicates that the transition from the G1 to S phase is impeded on microrough surfaces with a higher percentage of cyclin D1-positive cells. This provides a multifaceted explanation for the inhibitory mechanism of cell proliferation driven by the co-expression of the proliferation markers. This inhibitory activity on cell proliferation, typically seen on microrough surfaces, buttresses the general biological trade-off principle in osteoblasts positing the inverse correlation between the proliferation and differentiation.

Upregulated expression of ECM components such as collagen, laminin, fibronectin, and their corresponding adhesion molecules (integrins) were widely observed on microrough surfaces. This transcriptional observation was further bolstered by protein level analyses, showing increased production of collagen and fibronectin on microrough surfaces. Fibronectin is known to bind integrins, and an elevated expression of both suggests a coordinated response to enhance cell-substrate interactions [115,116]. These phenomena suggested that cells growing on microrough surfaces may display robust binding to the surrounding ECM and titanium surfaces via integrins. Traditionally, the principal advantage of microrough surfaces has been the promotion of mature bone formation around implants. The findings of this study propose that the distinct consequences of Rho family G-protein-mediated actin cytoskeleton organization and integrin-mediated augmented cell-ECM and cell-titanium surface connectivity could synergize to promote osteogenesis on roughened surfaces.

In addition to fibronectin, a similar trend was observed for other disulfide-linked or -targeted ECM or membranous glycoproteins such as laminin, CD36, and thrombospondin on microrough surfaces. Elemental sulfur is particularly found at bone-and-microrough titanium interfaces but not at bone-machined surface interfaces [13]. Enzymatic degradation of glycoproteins/proteoglycans within an osteoblastic culture on titanium induces the delamination of osteoblasts, suggesting the presence of sulfur-containing molecular glue in osseointegration [17,21,22]. The genes associated with disulfide-bonding may therefore play a key role in establishing the unique molecular interface between bone and microrough titanium.

Our strategy was to detect the genetic profile that builds molecular foundation for and triggers the accelerated osteoblast differentiation. It is very difficult and complicated to conduct RNA-seq in multiple groups at multiple time points. Therefore, we focused on the early stage of culture or osteoblast differentiation. ALP activity is an early-stage marker of osteoblast differentiation, followed by mid-stage makers such as collagen I, osteopontin, and later markers, such as osteocalcin and matrix mineralization. We attempted to choose a culture day before the mid-stage markers were detected different between machined and

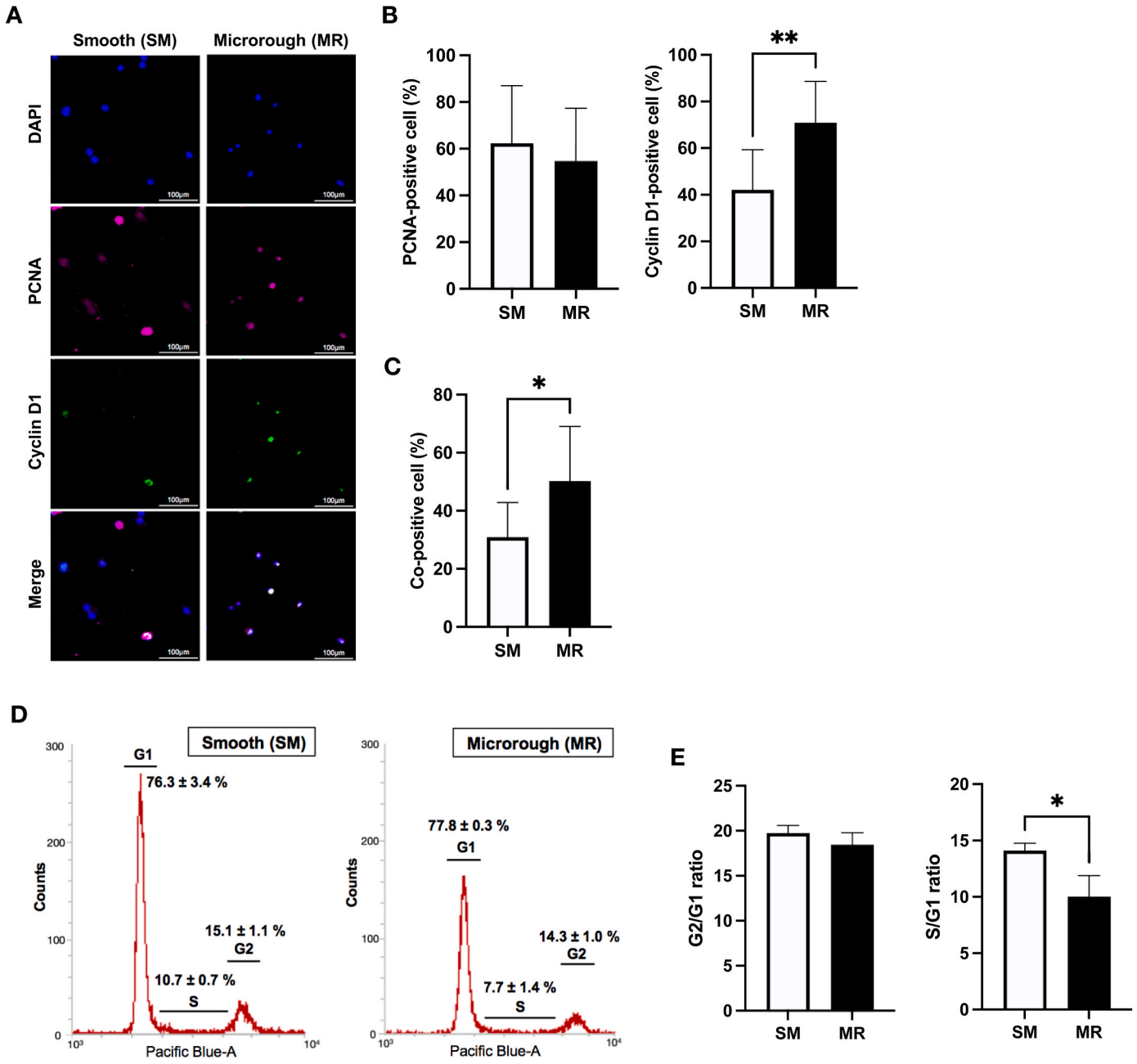

Fig. 8. PCNA and cyclin D1 expression of osteoblasts on different surface topographies. (A) Representative immunofluorescence images showing PCNA and cyclin D1 expression after 24 h of culture on smooth and microrough surfaces. (B) Quantitative evaluation of the proportion of PCNA-positive cells and cyclin D1-positive cells. (C) Ratio of cells co-expressing PCNA and cyclin D1. Data are presented as mean ± SD (n = 10). (D) Representative histograms showing the distribution of osteoblasts through cell cycle phases on day 5, with quantified distributions for each phase. (E) Quantification of the G2/G1 and S/G1 ratios between the different surfaces. Data are presented as mean ± SD (n = 3). *P < 0.05, **P < 0.005.

microrough surfaces and simultaneously needed to confirm the onset of surface-induced functional modulation. ALP activity started to show a difference between the two topographies on day 5 and the collagen 1 was expressed different on day 7 but not on day 5. Therefore, day 5 of culture was chosen for RNA-seq.

Our study was conducted under the controlled *in vitro* conditions. This approach, while enabling a focused exploration of a single type of cells, may not fully capture the complexity of *in vivo* osseointegration where other cell types, including blood and immune cells, proteins and cytokines, and other local and systemic factors are involved and interacted. Indeed, distinct blood clot formation, platelet interaction, and fibrin attachment on microrough surfaces reportedly are the contributing factors to faster osseointegration [117–120], which has not been addressed in the present study. The limitation of the present study also arises from a single time point of RNA-seq. Although we believed the initial culture stage is most critical to differentiate the biological process, subsequent stages of culture/differentiation may also be important to analyze because they may hold a key to determine bone formation and maturation on microrough surfaces. Based on the successful identification of distinct genetic profiles in the present study, further *in vitro* and *in vivo* RNA-seq studies are required.

5. Conclusions

This study represents the first genome-wide transcriptional profiling using RNA-seq to elucidate the impact of titanium surface topography on

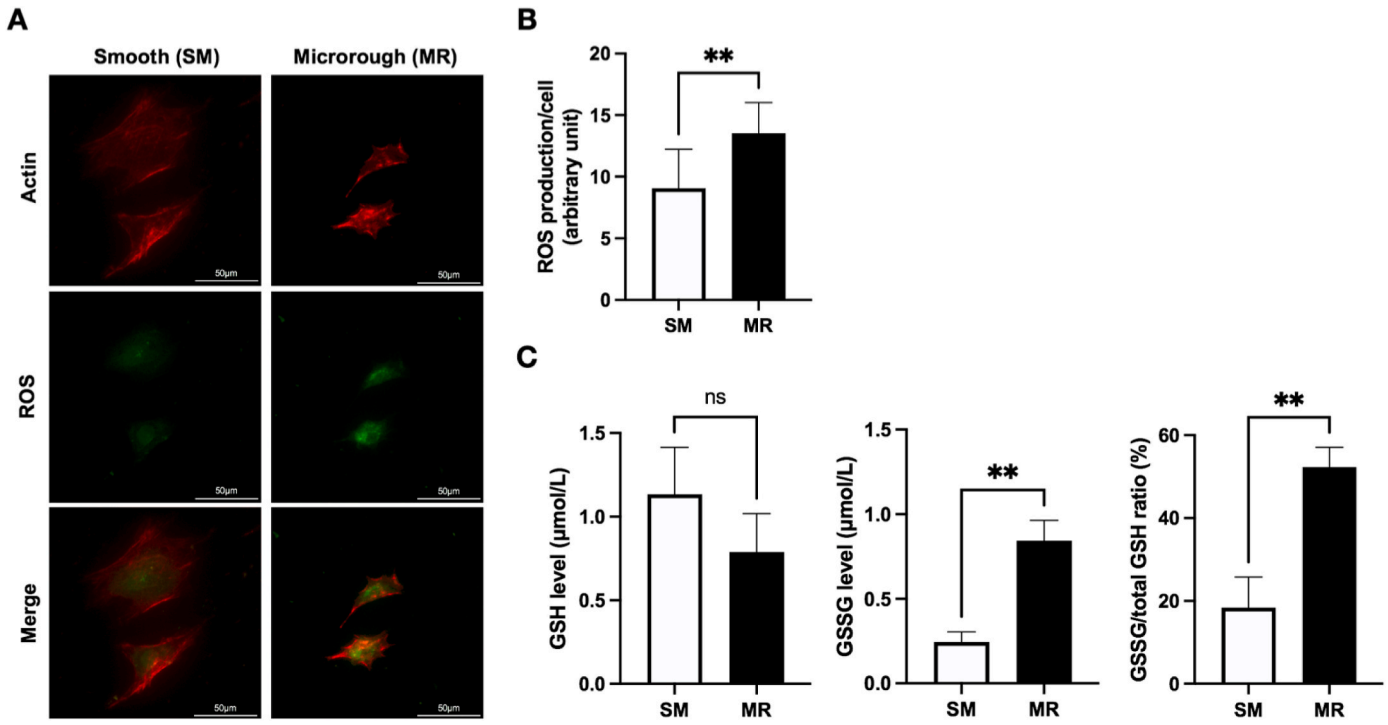

Fig. 9. Cellular stress responses to smooth and microrough surfaces after 24 h of culture. (A) Representative fluorescent microscopic images of osteoblasts, displaying ROS. (B) Quantitative analysis of intracellular ROS based on fluorescence intensity. Data are presented as mean ± SD (n = 10). (C) Measurement of glutathione (GSH) levels, oxidized glutathione (GSSG) levels, and the GSSG/total GSH ratio in osteoblasts. Data are presented as mean ± SD (n = 3). **P < 0.005.

osteoblast responses. Microrough surfaces modulate numerous cellular functions, including immune responses, stress responses, proliferation regulation, and cytoskeletal signaling. In particular, insightful information has been obtained implying molecular mechanisms associated with the promoted differentiation, reduced proliferation, distinct spreading behavior, and intracellular stress response of osteoblasts on microrough titanium surfaces. These molecular biological findings lay the groundwork for future research aimed at optimizing titanium surface modifications and advancing therapeutic strategies in the field of implantology.

Declaration of competing interest

The authors declare that they have no known competing financial interests or personal relationships that could have appeared to influence the work reported in this paper.

Data availability

Data will be made available on request.

Acknowledgments

This work was partially supported by the Division Research Fund (Division of Regenerative and Reconstructive Sciences).

Appendix A. Supplementary data

Supplementary data to this article can be found online at https://doi.org/10.1016/j.mtbio.2023.100852.

References

[1] D.D. Bosshardt, V. Chappuis, D. Buser, Osseointegration of titanium, titanium alloy and zirconia dental implants: current knowledge and open questions, Periodontol 73 (1) (2000) 22–40, 2017.
[2] T. Albrektsson, A. Wennerberg, On osseointegration in relation to implant surfaces, Clin. Implant Dent. Relat. Res. 21 (Suppl 1) (2019) 4–7.
[3] A. Wennerberg, T. Albrektsson, Effects of titanium surface topography on bone integration: a systematic review, Clin. Oral Implants Res. 20 (Suppl 4) (2009) 172–184.
[4] L.F. Cooper, Biologic determinants of bone formation for osseointegration: clues for future clinical improvements, J. Prosthet. Dent 80 (4) (1998) 439–449.
[5] G. Mendonça, D.B. Mendonça, F.J. Aragão, L.F. Cooper, Advancing dental implant surface technology–from micron- to nanotopography, Biomaterials 29 (28) (2008) 3822–3835.
[6] T. Albrektsson, A. Wennerberg, Oral implant surfaces: Part 1–review focusing on topographic and chemical properties of different surfaces and in vivo responses to them, Int. J. Prosthodont. (IJP) 17 (5) (2004) 536–543.
[7] A. Wennerberg, T. Albrektsson, On implant surfaces: a review of current knowledge and opinions, Int. J. Oral Maxillofac. Implants 25 (1) (2010) 63–74.
[8] T. Ogawa, I. Nishimura, Different bone integration profiles of turned and acid-etched implants associated with modulated expression of extracellular matrix genes, Int. J. Oral Maxillofac. Implants 18 (2) (2003) 200–210.
[9] T. Masuda, P.K. Yliheikkilä, D.A. Felton, L.F. Cooper, Generalizations regarding the process and phenomenon of osseointegration. Part I. In vivo studies, Int. J. Oral Maxillofac. Implants 13 (1) (1998) 17–29.
[10] K. Gotfredsen, L. Nimb, E. Hjörting-Hansen, J.S. Jensen, A. Holmén, Histomorphometric and removal torque analysis for TiO2-blasted titanium implants. An experimental study on dogs, Clin. Oral Implants Res. 3 (2) (1992) 77–84.
[11] A. Wennerberg, T. Albrektsson, B. Andersson, J.J. Krol, A histomorphometric and removal torque study of screw-shaped titanium implants with three different surface topographies, Clin. Oral Implants Res. 6 (1) (1995) 24–30.
[12] P. Trisi, R. Lazzara, A. Rebaudi, W. Rao, T. Testori, S.S. Porter, Bone-implant contact on machined and dual acid-etched surfaces after 2 months of healing in the human maxilla, J. Periodontol. 74 (7) (2003) 945–956.
[13] T. Ogawa, S. Ozawa, J.H. Shih, K.H. Ryu, C. Sukotjo, J.M. Yang, I. Nishimura, Biomechanical evaluation of osseous implants having different surface topographies in rats, J. Dent. Res. 79 (11) (2000) 1857–1863.
[14] F. Butz, T. Ogawa, I. Nishimura, Interfacial shear strength of endosseous implants, Int. J. Oral Maxillofac. Implants 26 (4) (2011) 746–751.
[15] M. Yamada, T. Ueno, H. Minamikawa, T. Ikeda, K. Nakagawa, T. Ogawa, Early-stage osseointegration capability of a submicrofeatured titanium surface created by microroughening and anodic oxidation, Clin. Oral Implants Res. 24 (9) (2013) 991–1001.
[16] T. Ogawa, C. Sukotjo, I. Nishimura, Modulated bone matrix-related gene expression is associated with differences in interfacial strength of different implant surface roughness, J. Prosthodont. 11 (4) (2002) 241–247.
[17] K. Takeuchi, L. Saruwatari, H.K. Nakamura, J.M. Yang, T. Ogawa, Enhanced intrinsic biomechanical properties of osteoblastic mineralized tissue on roughened titanium surface, J. Biomed. Mater. Res. 72 (3) (2005) 296–305.

[18] L.F. Cooper, T. Masuda, P.K. Yliheikkilä, D.A. Felton, Generalizations regarding the process and phenomenon of osseointegration. Part II. In vitro studies, Int. J. Oral Maxillofac. Implants 13 (2) (1998) 163–174.
[19] F. Butz, H. Aita, K. Takeuchi, T. Ogawa, Enhanced mineralized tissue adhesion to titanium over polystyrene assessed by the nano-scratch test, J. Biomed. Mater. Res. 74 (2) (2005) 164–170.
[20] F. Butz, H. Aita, C.J. Wang, T. Ogawa, Harder and stiffer bone osseointegrated to roughened titanium, J. Dent. Res. 85 (6) (2006) 560–565.
[21] H. Nakamura, J. Shim, F. Butz, H. Aita, V. Gupta, T. Ogawa, Glycosaminoglycan degradation reduces mineralized tissue-titanium interfacial strength, J. Biomed. Mater. Res. 77 (3) (2006) 478–486.
[22] H.K. Nakamura, F. Butz, L. Saruwatari, T. Ogawa, A role for proteoglycans in mineralized tissue-titanium adhesion, J. Dent. Res. 86 (2) (2007) 147–152.
[23] J. Shim, H. Nakamura, T. Ogawa, V. Gupta, An understanding of the mechanism that promotes adhesion between roughened titanium implants and mineralized tissue, J. Biomech. Eng. 131 (5) (2009), 054503.
[24] J.Y. Martin, Z. Schwartz, T.W. Hummert, D.M. Schraub, J. Simpson, J. Lankford Jr., D.D. Dean, D.L. Cochran, B.D. Boyan, Effect of titanium surface roughness on proliferation, differentiation, and protein synthesis of human osteoblast-like cells (MG63), J. Biomed. Mater. Res. 29 (3) (1995) 389–401.
[25] K. Anselme, M. Bigerelle, B. Noel, E. Dufresne, D. Judas, A. Iost, P. Hardouin, Qualitative and quantitative study of human osteoblast adhesion on materials with various surface roughnesses, J. Biomed. Mater. Res. 49 (2) (2000) 155–166.
[26] H. Aita, N. Hori, M. Takeuchi, T. Suzuki, M. Yamada, M. Anpo, T. Ogawa, The effect of ultraviolet functionalization of titanium on integration with bone, Biomaterials 30 (6) (2009) 1015–1025.
[27] K. Kubo, N. Tsukimura, F. Iwasa, T. Ueno, L. Saruwatari, H. Aita, W.A. Chiou, T. Ogawa, Cellular behavior on TiO2 nanonodular structures in a micro-to-nanoscale hierarchy model, Biomaterials 30 (29) (2009) 5319–5329.
[28] N.M. Rezaei, M. Hasegawa, M. Ishijima, K. Nakhaei, T. Okubo, T. Taniyama, A. Ghassemi, T. Tahsili, W. Park, M. Hirota, T. Ogawa, Biological and osseointegration capabilities of hierarchically (meso-/micro-/nano-scale) roughened zirconia, Int. J. Nanomed. 13 (2018) 3381–3395.
[29] J. Saruta, R. Ozawa, T. Okubo, S.R. Taleghani, M. Ishijima, H. Kitajima, M. Hirota, T. Ogawa, Biomimetic zirconia with cactus-inspired meso-scale spikes and nano-trabeculae for enhanced bone integration, Int. J. Mol. Sci. 22 (15) (2021).
[30] J. Saruta, N. Sato, M. Ishijima, T. Okubo, M. Hirota, T. Ogawa, Disproportionate effect of sub-micron topography on osteoconductive capability of titanium, Int. J. Mol. Sci. 20 (16) (2019).
[31] W. Att, K. Kubo, M. Yamada, H. Maeda, T. Ogawa, Biomechanical properties of jaw periosteum-derived mineralized culture on different titanium topography, Int. J. Oral Maxillofac. Implants 24 (5) (2009) 831–841.
[32] J.W. Park, Y.J. Kim, J.H. Jang, T.G. Kwon, Y.C. Bae, J.Y. Suh, Effects of phosphoric acid treatment of titanium surfaces on surface properties, osteoblast response and removal of torque forces, Acta Biomater. 6 (4) (2010) 1661–1670.
[33] H. Nakamura, L. Saruwatari, H. Aita, K. Takeuchi, T. Ogawa, Molecular and biomechanical characterization of mineralized tissue by dental pulp cells on titanium, J. Dent. Res. 84 (6) (2005) 515–520.
[34] T. Ikeda, Y. Hagiwara, M. Hirota, M. Tabuchi, M. Yamada, Y. Sugita, T. Ogawa, Effect of photofunctionalization on fluoride-treated nanofeatured titanium, J. Biomater. Appl. 28 (8) (2014) 1200–1212.
[35] F. Iwasa, N. Tsukimura, Y. Sugita, R.K. Kanuru, K. Kubo, H. Hasnain, W. Att, T. Ogawa, TiO2 micro-nano-hybrid surface to alleviate biological aging of UV-photofunctionalized titanium, Int. J. Nanomed. 6 (2011) 1327–1341.
[36] T. Ogawa, L. Saruwatari, K. Takeuchi, H. Aita, N. Ohno, Ti nano-nodular structuring for bone integration and regeneration, J. Dent. Res. 87 (8) (2008) 751–756.
[37] I. Nishimura, Y. Huang, F. Butz, T. Ogawa, A. Lin, C.J. Wang, Discrete deposition of hydroxyapatite nanoparticles on a titanium implant with predisposing substrate microtopography accelerated osseointegration, Nanotechnology 18 (24) (2007), 245101.
[38] H. Aita, W. Att, T. Ueno, M. Yamada, N. Hori, F. Iwasa, N. Tsukimura, T. Ogawa, Ultraviolet light-mediated photofunctionalization of titanium to promote human mesenchymal stem cell migration, attachment, proliferation and differentiation, Acta Biomater. 5 (8) (2009) 3247–3257.
[39] W. Att, N. Hori, F. Iwasa, M. Yamada, T. Ueno, T. Ogawa, The effect of UV-photofunctionalization on the time-related bioactivity of titanium and chromium-cobalt alloys, Biomaterials 30 (26) (2009) 4268–4276.
[40] T. Ogawa, Ultraviolet photofunctionalization of titanium implants, Int. J. Oral Maxillofac. Implants 29 (1) (2014) e95–e102.
[41] T. Suzuki, K. Kubo, N. Hori, M. Yamada, N. Kojima, Y. Sugita, H. Maeda, T. Ogawa, Nonvolatile buffer coating of titanium to prevent its biological aging and for drug delivery, Biomaterials 31 (18) (2010) 4818–4828.
[42] M. Hirota, Y. Sugita, M. Ishijima, T. Ikeda, J. Saruta, H. Maeda, T. Ogawa, UV photocatalytic activity of titanium dioxide (TiO2) surface contaminated with bacterial biofilm: implications for photo-restoration of osteoconductivity, Materials Today Advances 12 (2021), 100182.
[43] L. Saruwatari, H. Aita, F. Butz, H.K. Nakamura, J. Ouyang, Y. Yang, W.A. Chiou, T. Ogawa, Osteoblasts generate harder, stiffer, and more delamination-resistant mineralized tissue on titanium than on polystyrene, associated with distinct tissue micro- and ultrastructure, J. Bone Miner. Res. 20 (11) (2005) 2002–2016.
[44] N. Tsukimura, N. Kojima, K. Kubo, W. Att, K. Takeuchi, Y. Kameyama, H. Maeda, T. Ogawa, The effect of superficial chemistry of titanium on osteoblastic function, J. Biomed. Mater. Res. 84 (1) (2008) 108–116.
[45] M. Yamada, T. Ueno, N. Tsukimura, T. Ikeda, K. Nakagawa, N. Hori, T. Suzuki, T. Ogawa, Bone integration capability of nanopolymorphic crystalline hydroxyapatite coated on titanium implants, Int. J. Nanomed. 7 (2012) 859–873.
[46] X. Wei, W. Zhou, Z. Tang, H. Wu, Y. Liu, H. Dong, N. Wang, H. Huang, S. Bao, L. Shi, X. Li, Y. Zheng, Z. Guo, Magnesium surface-activated 3D printed porous PEEK scaffolds for in vivo osseointegration by promoting angiogenesis and osteogenesis, Bioact. Mater. 20 (2023) 16–28.
[47] T. Ma, C.X. Wang, X.Y. Ge, Y. Zhang, Applications of Polydopamine in Implant Surface Modification, Macromol Biosci, 2023, e2300067.
[48] J. Guillem-Marti, M. Gelabert, A. Heras-Parets, M. Pegueroles, M.P. Ginebra, J. M. Manero, RGD mutation of the heparin binding II fragment of fibronectin for guiding mesenchymal stem cell behavior on titanium surfaces, ACS Appl. Mater. Interfaces 11 (4) (2019) 3666–3678.
[49] M. Ishijima, A. Ghassemi, P. Soltanzadeh, M. Tanaka, K. Nakhaei, W. Park, M. Hirota, N. Tsukimura, T. Ogawa, Effect of UV photofunctionalization on osseointegration in aged rats, Implant Dent. 25 (6) (2016) 744–750.
[50] M. Ishijima, P. Soltanzadeh, M. Hirota, N. Tsukimura, T. Shigami, T. Ogawa, Enhancing osteoblast-affinity of titanium scaffolds for bone engineering by use of ultraviolet light treatment, Biomed. Res. 36 (1) (2015) 55–62.
[51] S.W. Kim, T. Ogawa, Y. Tabata, I. Nishimura, Efficacy and cytotoxicity of cationic-agent-mediated nonviral gene transfer into osteoblasts, J. Biomed. Mater. Res. 71 (2) (2004) 308–315.
[52] K. Hamajima, R. Ozawa, J. Saruta, M. Saita, H. Kitajima, S.R. Taleghani, D. Usami, D. Goharian, M. Uno, K. Miyazawa, S. Goto, K. Tsukinoki, T. Ogawa, The effect of TBB, as an initiator, on the biological compatibility of PMMA/MMA bone cement, Int. J. Mol. Sci. 21 (11) (2020).
[53] K. Komatsu, K. Hamajima, R. Ozawa, H. Kitajima, T. Matsuura, T. Ogawa, Novel tuning of PMMA orthopedic bone cement using TBB initiator: effect of bone cement extracts on bioactivity of osteoblasts and osteoclasts, Cells 11 (24) (2022).
[54] W. Att, N. Tsukimura, T. Suzuki, T. Ogawa, Effect of supramicron roughness characteristics produced by 1- and 2-step acid etching on the osseointegration capability of titanium, Int. J. Oral Maxillofac. Implants 22 (5) (2007) 719–728.
[55] C. Koyama, M. Hirota, Y. Okamoto, T. Iwai, T. Ogawa, T. Hayakawa, K. Mitsudo, A nitrogen-containing bisphosphonate inhibits osteoblast attachment and impairs bone healing in bone-compatible scaffold, J. Mech. Behav. Biomed. Mater. 104 (2020), 103635.
[56] T. Okubo, T. Ikeda, J. Saruta, N. Tsukimura, M. Hirota, T. Ogawa, Compromised epithelial cell attachment after polishing titanium surface and its restoration by UV treatment, Materials 13 (18) (2020).
[57] T. Matsuura, K. Komatsu, T. Ogawa, N-acetyl cysteine-mediated improvements in dental restorative material biocompatibility, Int. J. Mol. Sci. 23 (24) (2022).
[58] T. Taniyama, J. Saruta, N. Mohammadzadeh Rezaei, K. Nakhaei, A. Ghassemi, M. Hirota, T. Okubo, T. Ikeda, Y. Sugita, M. Hasegawa, T. Ogawa, UV-photofunctionalization of titanium promotes mechanical anchorage in A rat osteoporosis model, Int. J. Mol. Sci. 21 (4) (2020).
[59] T. Matsuura, K. Komatsu, D. Chao, Y.C. Lin, N. Oberoi, K. McCulloch, J. Cheng, D. Orellana, T. Ogawa, Cell type-specific effects of implant provisional restoration materials on the growth and function of human fibroblasts and osteoblasts, Biomimetics 7 (4) (2022).
[60] P. Limraksasin, P. Nattasit, J. Manokawinchoke, W. Tiskratok, N. Vinaikosol, H. Okawa, C.N. Limjeerajarus, N. Limjeerajarus, P. Pavasant, T. Osathanon, H. Egusa, Application of shear stress for enhanced osteogenic differentiation of mouse induced pluripotent stem cells, Sci. Rep. 12 (1) (2022), 19021.
[61] C. Prieto, D. Barrios, RaNA-Seq: interactive RNA-Seq analysis from FASTQ files to functional analysis, Bioinformatics 36 (6) (March 2020) 1955–1956.
[62] S. Chen, Y. Zhou, Y. Chen, J. Gu, fastp: an ultra-fast all-in-one FASTQ preprocessor, Bioinformatics 34 (17) (2018) i884–i890.
[63] R. Patro, G. Duggal, M.I. Love, R.A. Irizarry, C. Kingsford, Salmon provides fast and bias-aware quantification of transcript expression, Nat. Methods 14 (4) (2017) 417–419.
[64] S.X. Ge, E.W. Son, R. Yao, iDEP: an integrated web application for differential expression and pathway analysis of RNA-Seq data, BMC Bioinf. 19 (1) (2018) 534.
[65] M.D. Robinson, D.J. McCarthy, G.K. Smyth, edgeR: a Bioconductor package for differential expression analysis of digital gene expression data, Bioinformatics 26 (1) (2010) 139–140.
[66] M.I. Love, W. Huber, S. Anders, Moderated estimation of fold change and dispersion for RNA-seq data with DESeq2, Genome Biol. 15 (12) (2014) 550.
[67] S.X. Ge, D. Jung, R. Yao, ShinyGO: a graphical gene-set enrichment tool for animals and plants, Bioinformatics 36 (8) (2020) 2628–2629.
[68] W. Luo, C. Brouwer, Pathview: an R/Bioconductor package for pathway-based data integration and visualization, Bioinformatics 29 (14) (2013) 1830–1831.
[69] F.M. Chen, X. Liu, Advancing biomaterials of human origin for tissue engineering, Prog. Polym. Sci. 53 (2016) 86–168.
[70] M. Darnell, L. Gu, D. Mooney, RNA-seq reveals diverse effects of substrate stiffness on mesenchymal stem cells, Biomaterials 181 (2018) 182–188.
[71] M. Darnell, A. O'Neil, A. Mao, L. Gu, L.L. Rubin, D.J. Mooney, Material microenvironmental properties couple to induce distinct transcriptional programs in mammalian stem cells, Proc. Natl. Acad. Sci. U. S. A. 115 (36) (2018) E8368–e8377.
[72] W. Meng, Y. Zhou, Y. Zhang, Q. Cai, L. Yang, B. Wang, Effects of hierarchical micro/nano-textured titanium surface features on osteoblast-specific gene expression, Implant Dent. 22 (6) (2013) 656–661.
[73] D.P. Oliveira, A. Palmieri, F. Carinci, C. Bolfarini, Gene expression of human osteoblasts cells on chemically treated surfaces of Ti-6Al-4V-ELI, Mater. Sci. Eng., C 51 (2015) 248–255.

[74] E. Velasco-Ortega, I. Fos-Parra, D. Cabanillas-Balsera, J. Gil, I. Ortiz-García, M. Giner, J. Bocio-Núñez, M.J. Montoya-García, Á. Jiménez-Guerra, Osteoblastic cell behavior and gene expression related to bone metabolism on different titanium surfaces, Int. J. Mol. Sci. 24 (4) (2023).
[75] W. Att, N. Hori, M. Takeuchi, J. Ouyang, Y. Yang, M. Anpo, T. Ogawa, Time-dependent degradation of titanium osteoconductivity: an implication of biological aging of implant materials, Biomaterials 30 (29) (2009) 5352–5363.
[76] E. Eisenbarth, D. Velten, K. Schenk-Meuser, P. Linez, V. Biehl, H. Duschner, J. Breme, H. Hildebrand, Interactions between cells and titanium surfaces, Biomol. Eng. 19 (2–6) (2002) 243–249.
[77] G.N. Thalji, S. Nares, L.F. Cooper, Early molecular assessment of osseointegration in humans, Clin. Oral Implants Res. 25 (11) (2014) 1273–1285.
[78] F. Carinci, S. Volinia, F. Pezzetti, F. Francioso, L. Tosi, A. Piattelli, Titanium-cell interaction: analysis of gene expression profiling, J. Biomed. Mater. Res. B Appl. Biomater. 66 (1) (2003) 341–346.
[79] N. Kojima, S. Ozawa, Y. Miyata, H. Hasegawa, Y. Tanaka, T. Ogawa, High-throughput gene expression analysis in bone healing around titanium implants by DNA microarray, Clin. Oral Implants Res. 19 (2) (2008) 173–181.
[80] D. Yin, S. Komasa, S. Yoshimine, T. Sekino, J. Okazaki, Effect of mussel adhesive protein coating on osteogenesis in vitro and osteointegration in vivo to alkali-treated titanium with nanonetwork structures, Int. J. Nanomed. 14 (2019) 3831–3843.
[81] J.K. Leach, J. Whitehead, Materials-directed differentiation of mesenchymal stem cells for tissue engineering and regeneration, ACS Biomater. Sci. Eng. 4 (4) (2018) 1115–1127.
[82] J. Li, R. Hou, X. Niu, R. Liu, Q. Wang, C. Wang, X. Li, Z. Hao, G. Yin, K. Zhang, Comparison of microarray and RNA-Seq analysis of mRNA expression in dermal mesenchymal stem cells, Biotechnol. Lett. 38 (1) (2016) 33–41.
[83] S. Zhao, W.P. Fung-Leung, A. Bittner, K. Ngo, X. Liu, Comparison of RNA-Seq and microarray in transcriptome profiling of activated T cells, PLoS One 9 (1) (2014), e78644.
[84] M.S. Rao, T.R. Van Vleet, R. Ciurlionis, W.R. Buck, S.W. Mittelstadt, E.A. G. Blomme, M.J. Liguori, Comparison of RNA-seq and microarray gene expression platforms for the toxicogenomic evaluation of liver from short-term rat toxicity studies, Front. Genet. 9 (2018) 636.
[85] R. Du, C. Huang, K. Liu, X. Li, Z. Dong, Targeting AURKA in Cancer: molecular mechanisms and opportunities for Cancer therapy, Mol. Cancer 20 (1) (2021) 15.
[86] X. Li, S. Wei, S. Niu, X. Ma, H. Li, M. Jing, Y. Zhao, Network pharmacology prediction and molecular docking-based strategy to explore the potential mechanism of Huanglian Jiedu Decoction against sepsis, Comput. Biol. Med. 144 (2022), 105389.
[87] M.J. Dalby, D. McCloy, M. Robertson, H. Agheli, D. Sutherland, S. Affrossman, R. O. Oreffo, Osteoprogenitor response to semi-ordered and random nanotopographies, Biomaterials 27 (15) (2006) 2980–2987.
[88] M.J. Biggs, R.G. Richards, M.J. Dalby, Nanotopographical modification: a regulator of cellular function through focal adhesions, Nanomedicine 6 (5) (2010) 619–633.
[89] M.J. Dalby, N. Gadegaard, R. Tare, A. Andar, M.O. Riehle, P. Herzyk, C. D. Wilkinson, R.O. Oreffo, The control of human mesenchymal cell differentiation using nanoscale symmetry and disorder, Nat. Mater. 6 (12) (2007) 997–1003.
[90] X. Yang, G. Wang, X. Huang, M. Cheng, Y. Han, RNA-seq reveals the diverse effects of substrate stiffness on epidermal ovarian cancer cells, Aging (Albany NY) 12 (20) (2020) 20493–20511.
[91] T. Ogawa, I. Nishimura, Genes differentially expressed in titanium implant healing, J. Dent. Res. 85 (6) (2006) 566–570.
[92] S. Muralidharan, P. Mandrekar, Cellular stress response and innate immune signaling: integrating pathways in host defense and inflammation, J. Leukoc. Biol. 94 (6) (2013) 1167–1184.
[93] T. Ueno, T. Ikeda, N. Tsukimura, M. Ishijima, H. Minamikawa, Y. Sugita, M. Yamada, N. Wakabayashi, T. Ogawa, Novel antioxidant capability of titanium induced by UV light treatment, Biomaterials 108 (2016) 177–186.
[94] E.A. Lewallen, W.H. Trousdale, R. Thaler, J.J. Yao, W. Xu, J.M. Denbeigh, A. Nair, J.P. Kocher, A. Dudakovic, D.J. Berry, R.C. Cohen, M.P. Abdel, D.G. Lewallen, A. J. van Wijnen, Surface roughness of titanium orthopedic implants alters the biological phenotype of human mesenchymal stromal cells, Tissue Eng. 27 (23–24) (2021) 1503–1516.
[95] N. Sato, K. Kubo, M. Yamada, N. Hori, T. Suzuki, H. Maeda, T. Ogawa, Osteoblast mechanoresponses on Ti with different surface topographies, J. Dent. Res. 88 (9) (2009) 812–816.
[96] D.S. Amarasekara, S. Kim, J. Rho, Regulation of osteoblast differentiation by cytokine networks, Int. J. Mol. Sci. 22 (6) (2021).
[97] A. Greenbaum, Y.M. Hsu, R.B. Day, L.G. Schuettpelz, M.J. Christopher, J. N. Borgerding, T. Nagasawa, D.C. Link, CXCL12 in early mesenchymal progenitors is required for haematopoietic stem-cell maintenance, Nature 495 (7440) (2013) 227–230.
[98] O. Omar, M. Lennerås, S. Svensson, F. Suska, L. Emanuelsson, J. Hall, U. Nannmark, P. Thomsen, Integrin and chemokine receptor gene expression in implant-adherent cells during early osseointegration, J. Mater. Sci. Mater. Med. 21 (3) (2010) 969–980.
[99] S. Otsuru, K. Tamai, T. Yamazaki, H. Yoshikawa, Y. Kaneda, Circulating bone marrow-derived osteoblast progenitor cells are recruited to the bone-forming site by the CXCR4/stromal cell-derived factor-1 pathway, Stem Cell. 26 (1) (2008) 223–234.
[100] X. Rausch-fan, Z. Qu, M. Wieland, M. Matejka, A. Schedle, Differentiation and cytokine synthesis of human alveolar osteoblasts compared to osteoblast-like cells (MG63) in response to titanium surfaces, Dent. Mater. 24 (1) (2008) 102–110.
[101] G. Zhao, Z. Schwartz, M. Wieland, F. Rupp, J. Geis-Gerstorfer, D.L. Cochran, B. D. Boyan, High surface energy enhances cell response to titanium substrate microstructure, J. Biomed. Mater. Res. 74 (1) (2005) 49–58.
[102] A.R. Harris, P. Jreij, D.A. Fletcher, Mechanotransduction by the actin cytoskeleton: converting mechanical stimuli into biochemical signals, Annu. Rev. Biophys. 47 (1) (2018) 617–631.
[103] N. Wang, Review of cellular mechanotransduction, J. Phys. D Appl. Phys. 50 (23) (2017).
[104] F. Iwasa, K. Baba, T. Ogawa, Enhanced intracellular signaling pathway in osteoblasts on ultraviolet lighttreated hydrophilic titanium, Biomed. Res. 37 (1) (2016) 1–11.
[105] K. Anselme, P. Linez, M. Bigerelle, D. Le Maguer, A. Le Maguer, P. Hardouin, H. F. Hildebrand, A. Iost, J.M. Leroy, The relative influence of the topography and chemistry of TiAl6V4 surfaces on osteoblastic cell behaviour, Biomaterials 21 (15) (2000) 1567–1577.
[106] D. De Santis, C. Guerriero, P.F. Nocini, A. Ungersbock, G. Richards, P. Gotte, U. Armato, Adult human bone cells from jaw bones cultured on plasma-sprayed or polished surfaces of titanium or hydroxylapatite discs, J. Mater. Sci. Mater. Med. 7 (1) (1996) 21–28.
[107] E.M. Boehm, M.S. Gildenberg, M.T. Washington, The many roles of PCNA in eukaryotic DNA replication, Enzymes 39 (2016) 231–254.
[108] A. González-Magaña, F.J. Blanco, Human PCNA structure, function and interactions, Biomolecules 10 (4) (2020).
[109] G.L. Moldovan, B. Pfander, S. Jentsch, PCNA, the maestro of the replication fork, Cell 129 (4) (2007) 665–679.
[110] P. Ramos-García, J.A. Gil-Montoya, C. Scully, A. Ayén, L. González-Ruiz, F. J. Navarro-Triviño, M.A. González-Moles, An update on the implications of cyclin D1 in oral carcinogenesis, Oral Dis. 23 (7) (2017) 897–912.
[111] G. Tchakarska, B. Sola, The double dealing of cyclin D1, Cell Cycle 19 (2) (2020) 163–178.
[112] J. Fukami-Kobayashi, Y. Mitsui, Cyclin D1 inhibits cell proliferation through binding to PCNA and cdk2, Exp. Cell Res. 246 (2) (1999) 338–347.
[113] K. Yang, M. Hitomi, D.W. Stacey, Variations in cyclin D1 levels through the cell cycle determine the proliferative fate of a cell, Cell Div. 1 (1) (2006) 32.
[114] Y. Xiong, H. Zhang, D. Beach, D type cyclins associate with multiple protein kinases and the DNA replication and repair factor PCNA, Cell 71 (3) (1992) 505–514.
[115] M. Barczyk, S. Carracedo, D. Gullberg, Integrins, Cell Tissue Res 339 (1) (2010) 269–280.
[116] N. Hogg, R. Henderson, B. Leitinger, A. McDowall, J. Porter, P. Stanley, Mechanisms contributing to the activity of integrins on leukocytes, Immunol. Rev. 186 (2002) 164–171.
[117] J.E. Davies, In vitro modeling of the bone/implant interface, Anat. Rec. 245 (2) (1996) 426–445.
[118] J.E. Davies, Mechanisms of endosseous integration, Int. J. Prosthodont. (IJP) 11 (5) (1998) 391–401.
[119] J.E. Davies, Understanding peri-implant endosseous healing, J. Dent. Educ. 67 (8) (2003) 932–949.
[120] L. Kikuchi, J.Y. Park, C. Victor, J.E. Davies, Platelet interactions with calcium-phosphate-coated surfaces, Biomaterials 26 (26) (2005) 5285–5295.